Modeling corticotroph deficiency with pituitary organoids supports the functional role of *NFKB2* in human pituitary differentiation

Authors

Thi Thom Mac[1, 2], Teddy Fauquier[1], Nicolas Jullien[3], Pauline Romanet[1, 4], Heather C. Etchevers[1], Anne Barlier[1, 4, 5], Frederic Castinetti[1, 5], Thierry Brue[1, 5]*

(1) Aix Marseille Univ, INSERM, UMR1251, Marseille Medical Genetics, Institut MarMaRa, Marseille, France

(2) Endocrinology Department, Hanoi Medical University Hospital, Hanoi, Vietnam

(3) Aix Marseille Univ, CNRS, UMR7051, Institut de NeuroPhysiopathologie, Marseille, France

(4) Aix Marseille Univ, APHM, INSERM, MMG, Laboratory of Molecular Biology, La Conception Hospital, Institut MarMaRa, Marseille, France

(5) Aix Marseille Univ, APHM, INSERM, MMG, Department of Endocrinology, La Conception Hospital, Institut MarMaRa, Marseille, France

Keywords

Congenital hypopituitarism, DAVID syndrome, hiPSC, CRISPR/Cas9, organoids, hypothalamic-pituitary organoids, NFKB2, anterior pituitary deficiency, ACTH deficiency, corticotroph differentiation, stem cell, development, hypogammaglobulinemia, CVID, variable immunodeficiency

22

23

24 *** Corresponding author**

25 Prof. Thierry Brue, La Conception Hospital, Department of Endocrinology, 147

26 boulevard Baille, 13005 Marseille, France; thierry.brue@ap-hm.fr

Abstract

Background: Deficient Anterior pituitary with common Variable Immune Deficiency (DAVID) syndrome is a rare condition characterized by the association of adrenocorticotropic hormone deficiency (ACTHD) and primary hypogammaglobulinemia, caused by *NFKB2* heterozygous mutations. Nuclear factor kappa B (NFKB) signaling is a key regulator of the immune system; however, the underlying mechanism of its association with endocrine symptoms remains unknown. Two main hypotheses explain the effects of mutant NFKB2 on the pituitary gland: an autoimmune hypophysitis, preferentially affecting corticotroph function, or a primary developmental defect. The role of NFKB2 in the development of the human pituitary was called into question by *Nfkb2*-deficient *Lym1* mice, which have normal pituitary functions.

Purpose: The aim of this study was to create a human disease model to define the role of *NFKB2* in human pituitary development.

Methods: We established pituitary organoids in three dimensions (3D) culture after directed differentiation from CRISPR/Cas9-edited human induced pluripotent stem cells (hiPSC). First, we conducted a proof-of-concept study, introducing a homozygous $TBX19^{K146R/K146R}$ missense pathogenic variant in hiPSC, an allele found in patients with congenital isolated ACTHD. Then, we used the same method to produce $NFKB2^{D865G/D865G}$ mutant organoids, harboring the pathogenic missense variant previously identified in DAVID patients. This mutation causes a failure of NFKB2 p100 phosphorylation that blocks processing to form active NFKB2 p52. We then characterized pituitary organoid development by transcriptomics using bulk RNA sequencing and quantitative RT-PCR, and by immunofluorescence in section and whole-mount.

Results: Analysis of wild-type (WT) organoids demonstrated that this *in vitro* model recapitulates corticotroph cell differentiation. *TBX19*$^{K146R/K146R}$ organoids conserved early expression of *HESX1*, but had significantly decreased *PITX1*, *TBX19*, *LHX3,* and *POMC* transcription*.* *NFKB2*$^{D865G/D865G}$ organoids also had dramatically reduced corticotrophs. Furthermore, *NFKB2*$^{D865G/D865G}$ perturbs the normal expression of 66 genes known to contribute to pituitary development, among which 21 transcription factors.

Conclusions: We used a combination of CRISPR/Cas9 editing and refinement of a 3D organoid culture protocol to model human ACTHD due to *TBX19* or *NFKB2* mutations. The *NFKB2* variant studied induced a significant decrease in corticotroph differentiation, demonstrating for the first time a direct functional role of NFKB2 in human pituitary development. Signaling through NFKB2 is thus a valid new candidate pathway in the pathogenesis of isolated or syndromic ACTHD.

Introduction

Adrenocorticotropic hormone deficiency (ACTHD) is defined by an insufficient production of ACTH by the pituitary, followed by low adrenal cortisol production. Proper diagnosis and management of ACTHD is crucial, as it is a life-threatening condition in the neonatal period, characterized by hypoglycemia, cholestatic jaundice and seizures[1]. Constitutional ACTHD, which is diagnosed at birth or during the first years of life, can be isolated or associated with deficiencies in other pituitary hormones such as growth hormone (GH) or thyrotropin-stimulating hormone (TSH) and termed combined pituitary hormone deficiency (CPHD). ACTHD is genetically heterogeneous, due to mutations in genes coding mostly for transcription factors responsible for pituitary ontogenesis or their regulation. Responsible genes identified to date include the T-box transcription factor *TBX19* (also known as *TPIT*), *NFKB2, LHX3, LHX4, PROP1, HESX1, SOX2, SOX3, OTX2* and *FGF8*.

Mutations of *TBX19* account for approximately two-thirds of neonatal-onset complete isolated ACTHD[1]. TBX19 is a T-box transcription factor restricted to pituitary pro-opiomelanocortin (POMC)-expressing cells in mice and humans. It is essential for *POMC* gene transcription and terminal differentiation of POMC-expressing cells in the anterior pituitary (also known as the adenohypophysis)[2]. POMC is cleaved to produce ACTH in corticotroph cells. *TBX19*-deficient mice have only a few pituitary *POMC*-expressing cells, with very low ACTH and undetectable corticosterone levels[3]. In humans with isolated ACTH deficiency, *TBX19* mutations lead to loss-of-function by different mechanisms, such as the K146R (exon 2, c.437 A>G) pathogenic variant located in the T-box region, which results in a loss of DNA-binding ability[1].

Thanks to GENHYPOPIT[4–6], an international network aimed at identifying new genetic etiologies of combined pituitary hormone deficiency, we described the first

90 cases of DAVID (Deficient Anterior pituitary with common Variable Immune Deficiency)
91 syndrome, a rare association of hypopituitarism (mainly ACTHD) and immune
92 deficiency (hypogammaglobulinemia) [7]. DAVID syndrome is associated with variants in
93 the nuclear factor kappa-B subunit 2 (*NFKB2*) gene[8,9]. In particular, we reported that a
94 pathogenic, heterozygous D865G (exon 23, c.2594 A>G) *NFKB2* variant was found in a
95 patient presenting with severe recurrent infections from 2 years of age, who at the age
96 of 5 was diagnosed with ACTHD[7]. Mutations in the C-terminal region of NFKB2 lead to
97 the disruption of both non-canonical and canonical pathways[10–12].

98 Full-length NFKB2 (p100) protein has 2 critical serines, S866 and S870, in the C-
99 terminal domain. Phosphorylation of these sites yields the transcriptionally active form
100 of NFKB2 (p52) by enabling the proteasomal processing of the larger p100 protein. The
101 D865G mutation, located adjacent to the critical S866 phosphorylation site, protects
102 mutant protein from proteasomal degradation, causes defective processing of p100 to
103 p52, and results in reduced translocation of p52 to the nucleus[8,11,12]. *NFKB2*$^{D865G/+}$
104 resulted in half of the normal level of processing to p52, whereas *NFKB2*$^{D865G/D865G}$
105 exhibited near-absence of p52[12]. The nuclear factor kappa B (NFKB) signaling pathway
106 is a key regulator of the immune system[12–14], which likely explains the immune
107 phenotype of patients with DAVID syndrome, including susceptibility to infections and
108 auto-immune disorders[15]. In contrast, the underlying mechanism causing pituitary
109 disorders remains unknown, with two predominating hypotheses: an indirect
110 autoimmune hypophysitis, preferentially affecting corticotroph function, or a primary
111 developmental defect supported by the expression of *NFKB2* in the human fetal
112 pituitary[16]. However, a developmental role for NFKB2 was not confirmed in the *Lym1*
113 mouse model, carrying a heterozygous or homozygous nonsense variant Y868*, which
114 presented apparently normal pituitary development and function although impairing
115 immunity[9]. Although the mouse continues to be a relevant model for many aspects of

116 pituitary organ development, we sought a higher-throughput method to assess
117 pathogenic effects of new candidate genes or variants on human pituitary
118 differentiation.

119 Human induced pluripotent stem cell (hiPSC)-derived organoids have emerged
120 as promising models to study many developmental mechanisms and their perturbation
121 in disease[17]. Pioneering work on human embryonic stem cells and later, hiPSC,
122 established that 3D organoid models can replicate aspects of pituitary development[18–20],
123 and could thus be of major interest in modeling pituitary disorders[18,21,22]. In the present
124 study, we applied recent progress in genome editing using CRISPR/Cas9[23] to a refined
125 protocol to derive 3D organoids from hiPSC in order to model ACTHD. We validated the
126 recapitulation of corticotroph cell differentiation *in vitro* by introducing a *TBX19*
127 mutation known to induce isolated human ACTHD and documenting the subsequent
128 deficiencies in corticotroph development. When used to characterize the D865G *NFKB2*
129 variant found in patients with DAVID syndrome, hiPSC-derived pituitary organoids
130 displayed dramatically altered corticotroph differentiation in the absence of immune
131 cells, demonstrating for the first time a direct and incontrovertible role for NFKB2 in
132 human pituitary development.

133 **Materials and methods**

134 **Culture and maintenance of hiPSC lines**

135 The 10742L hiPSC line, derived from a healthy individual, was used in the study as the
136 WT control (characterized and provided by the Cell Reprogramming and Differentiation
137 Facility [MaSC], Marseille Medical Genetics, Marseille, France). Further information
138 about this line is indicated in **Suppl Table S1**. Two mutant lines carrying
139 *TBX19*$^{K146R/K146R}$ and *NFKB2*$^{D865G/D865G}$ were subsequently generated from 10742L using
140 CRISPR/Cas9 editing as described below. All hiPSC lines were cultured on six-well
141 plates (Corning, #3335, New York, USA) coated with Synthemax II-SC Substrate
142 (working concentration at 0.025 mg/mL, Corning, New York, USA) and maintained
143 undifferentiated in a chemically defined growth medium (StemMACs hiPSC-Brew XF ;
144 MACS Miltenyi Biotec, Paris, France)[24]. hiPSC lines were maintained in a humidified
145 incubator under conditions of 37°C, 5% CO_2, with a daily change of medium, and
146 passaged when cells reached 60-80 % confluency using enzyme-free ReleSR, according
147 to manufacturer recommendations (StemCell Technologies, Canada, #05872).

148 **CRISPR/Cas9 mediated genome editing of hiPSC**

149 CRISPR/Cas9 gene editing was used to introduce the *TBX19*$^{K146R/K146R}$ and the
150 *NFKB2*$^{D865G/D865G}$ mutations using a previously described method[25]. The *TBX19*$^{K146R/K146R}$
151 line harbored the c.437A>G, p.Lys146Arg *TBX19* (NM_005149) pathogenic missense
152 variant. The *NFKB2*$^{D865G/D865G}$ line harbored the c.2594A>G, p.Asp865Gly *NFKB2*
153 (NM_001322934) pathogenic missense variant.

154 *Preparation of the CRISPR/Cas9 sgRNA plasmid*

155 For each targeted gene, a sgRNA plasmid was prepared as previously described[26].
156 Briefly, we designed a sgRNA sequence within 20 nucleotides of the target site, selected
157 with the open-source CRISPOR tool (http://crispor.tefor.net/)[27].

158 The sgRNA sequence used to generate *TBX19*^{K146R} was (5'>3'):
159 AAGCTGACCAACAAGCTCAA (see also Table S2).
160 The sgRNA sequence used to generate *NFKB2*^{D865G} was (5'>3'):
161 GTGAAGGAAGACAGTGCGTA (see also Table S3).

162 We used the cAB03 (also known as pX459-pEF1alpha) vector as previously described[25].
163 In this, the pSpCas9 (BB)-2A-Puro (PX459) V2.0 (Addgene plasmid # 62988, Addgene,
164 Teddington, UK) was modified by an EF1alpha promoter[25]. The chosen sgRNA was
165 cloned into the cAB03 open plasmid vector as previously described by Arnaud et al[25].
166 The final vector expressed the corresponding sgRNA under the control of the U6
167 promoter, as well as *Cas9* under the control of the EF-1alpha promoter, and a
168 puromycin resistance gene.

169 *Single-stranded oligo DNA nucleotides (ssODN) design*

170 We also designed donor sequences to generate *TBX19*^{K146R} and *NFKB2*^{D865G} missense
171 mutations. A donor sequence is used for homology-directed repair, allowing the
172 introduction ("knock-in", KI) of single nucleotide variations with low efficiency. To
173 optimize the efficiency of KI editing, the donor sequences were designed as single-
174 stranded oligo DNA nucleotides (ssODN), carrying the mutation of interest, and also
175 included a silent (or blocking) mutation that mutates the protospacer-adjacent motif
176 (PAM) or disrupts the sgRNA binding region to prevent re-cutting by Cas9 after
177 successful editing[28,29,25,30]. The ssODN contained 100 nucleotides with homology arms
178 on each side of the target region. The ssODN sequences were as follows (see also **Suppl**
179 **Tables S2 – Table S3)**:

180 For *TBX19*^{K146R} (5'-3'):

181 TGGATGAAAGCTCCCATCTCCTTCAGCAAAGTGAGGCTGACCAACAAGTTAAATGGAGGCGG

182 GCAGGTACGAATGAGGCGGGCAGGCCTGGCCACCCGCT

183 For *NFKB2*^{D865G} (5'-3'):

184 TCCCATTCCTGTCCCCATTTACCCCCAGCAGAGGTGAAGGAAGGCAGTGCCTACGGGAGCCAG

185 TCAGTGGAGCAGGAGGCAGAGAAGCTGGGCCCACCCC.

186 ssODN were synthesized by Integrated DNA Technologies (Coralville, Iowa, US) at

187 Ultramer™ quality.

188 *Electroporation*

189 hiPSC were transfected with constructed sgRNA/Cas9 vectors by electroporation using

190 the Neon Transfection System 100 µL kit (Invitrogen). A summary of the procedure is

191 described in **Suppl. Figure S1**.

192 *Clone isolation and screening*

193 On day 3 post-transfection, we used the cleaved amplified polymorphic sequences

194 (CAPS) assay to estimate the efficacy of CRISPR/Cas9 in bulk transfected hiPSC

195 populations and to choose a number of colonies to be picked for further amplification[31].

196 A restriction enzyme recognition site was included in each donor template (BseI for

197 *TBX19* and MseI for *NFKB2*). CAPS primers and restriction enzymes were chosen

198 assisted by AmplifX software (version 2.0.0b3; https://inp.univ-amu.fr/en/amplifx-

199 manage-test-and-design-your-primers-for-pcr). CAPS primers are listed in **Suppl Table**

200 **S4**. The PCR reaction was performed using the PCR condition reported in **Suppl Table**

201 **S5 – Suppl Table S6**. The CAPS products were separated and visualized by

202 electrophoresis on a 2% agarose gel and analyzed for densitometry with ImageJ[25,30].

203 After 10 days, the CAPS assay was also used to screen and identify possible knock-in
204 (KI) clones. KI clones were then confirmed by Sanger sequencing (Genewiz, Leipzig,
205 Germany). Analyses of Sanger traces were made using Sequencher DNA sequence
206 analysis software (version 5.4.6, Gene Codes Corporation, Ann Arbor, MI USA,
207 http://www.genecodes.com) to align sequences of KI clones with WT sequence to
208 confirm the successful edition. Sanger sequencing primers are described in **Suppl Table**
209 **S4**. KI clones were amplified and then cryopreserved.

210 ***In vitro* pituitary organoids differentiated from hiPSC**

211 Pituitary organoids were produced in parallel using the same protocol for WT and
212 edited hiPSC lines. Two batches of differentiation with two hundred organoids for each
213 hiPSC line were generated, respectively WT versus *TBX19*$^{K146R/K146R}$ organoids or WT
214 versus *NFKB2*$^{D865G/D865G}$ organoids.

215 Differentiation was based on a protocol from Matsumoto et al. with some
216 modifications[20,22]. hiPSCs were first dissociated into single cells using Accutase. Ten
217 thousand cells per organoid were plated in 20 µL hanging drops under the lid of a 127.8
218 x 85,5mm single-well plate (Greiner bio-one) in growth factor-free, chemically defined
219 medium (gfCDM) supplemented with 10% (vol/vol) Knockout Serum Replacement
220 (KSR; Thermo Fisher Scientific, #10828-010) and 20 µM Y-27632 (Sigma-Aldrich, #
221 SCM75). The lid was inverted over the bottom chamber (filled with 10 mL of sterile
222 water to avoid the evaporation of droplets) and incubated at 37°C/5% CO_2 for 2 days.
223 Once aggregates formed, organoids were transferred to non-adhesive 100x20mm
224 culture dishes (Corning) containing 10 mL of gfCDM medium supplemented with 10%
225 KSR without Y-27632 and incubated at 37°C and 5% CO_2 until day 6. From days 6 to
226 days 17, the medium was supplemented with 10% KSR, 5 nM recombinant human bone
227 morphogenetic protein 4 (BMP4; Peprotech, # AF-120-05ET, USA) and 2 µM

228 Smoothened agonist (SAG; Sigma-Aldrich/Merck, # SML 1314). Half of the medium was
229 renewed every 2 - 3 days.

230 From day 18, BMP4 was withdrawn and half of the medium was renewed every 2 - 3
231 days. At this point, organoids were maintained under high-O_2 conditions (40%) and 5%
232 CO_2 in an MCO-5M incubator (Panasonic). From day 30, gfCDM medium supplemented
233 with 20% knockout serum replacement was used, and all medium was renewed every
234 2-3 days until at least day 105. Induction into pituitary progenitor cells (defined as
235 LHX3+) and into pituitary hormone-producing cells was evaluated by qRT-PCR (on days
236 0, 6, 18, 27, 48, 75, 105) and immunofluorescence (on days 48 and 105) (see below).

237 **Validating *TBX19*^{K146R} targeting and assessing off-target mutations by whole**
238 **genome sequencing (WGS)**

239 For *TBX19*^{K146R}, we used whole genome sequencing (WGS) to assess on-target and off-
240 target mutations, because the edited site is far from the cut site (15 bases). DNA
241 extracted from control and *TBX19*$^{K146R/K146R}$ (5 organoids each) was submitted for WGS
242 (Integragen Genomics platform). PCR-free libraries were prepared with the NEBNext
243 Ultra™ II DNA Library Prep Kits (New England BioLabs) according to supplier
244 recommendations. Specific double-strand gDNA quantification and a fragmentation
245 (300 ng of input with high-molecular-weight gDNA) sonication method were used to
246 obtain approximately 400 bp fragments. Finally, paired-end adaptor oligonucleotides
247 (xGen TS-LT Adapter Duplexes from Integrated DNA Technologies) were ligated and re-
248 paired. Tailed fragments were purified for direct sequencing without a PCR step. DNA
249 PCR free libraries were sequenced on paired-end 150 pb runs on the NovaSeq6000
250 (Illumina) apparatus. Image analysis and base calling were performed using Illumina
251 Real Time Analysis (RTA) Pipeline with default parameters. Sequence reads were
252 mapped on the Human Genome Build (GRCh38) using the Burrows-Wheeler Aligner

253 (BWA)[32]. Variant calling was performed via the GATK Haplotype Caller GVCF tool (GATK
254 3.8.1, Broad Institute)[33]. Mutation enrichment was determined using Fisher's Exact
255 Test. Variants were annotated with Ensembl's Variant Effect Predictor, VEP) by
256 Integragen Genomics[34]. These NGS analyses confirmed the presence of on-target
257 mutation and the absence of off-target mutation in the top four predicted off-target
258 sites.

259 **Validating *NFKB2^{D865G}* targeting, assessing off-target mutations and differential**
260 **expression analysis by bulk RNA sequencing (RNA-seq)**

261 For *NFKB2^{D865G}*, we used bulk RNA sequencing (RNA-seq) for analysis of differential
262 RNA expression, and to assess on-target and off-target mutations, because the target
263 site is close to the cleavage site (6 bases). A total of 500 ng of total RNA was extracted
264 from 10 individual organoids (5 *NFKB2$^{D865G/D865G}$* and 5 control organoids). RNA-seq
265 libraries were generated using the KAPA mRNA HyperPrep kit (Roche). The quality and
266 profile of the libraries were visualized on a Bioanalyzer using the High Sensitivity DNA
267 assay (Agilent) and-quantified on a Qubit using the dsDNA High Sensibility Kit (Thermo
268 Fisher Scientific). Finally, we performed 2x 76-bp paired-end sequencing on a
269 NextSeq500 (Illumina). After quality control using FastQC (Braham Institute), reads
270 were aligned on the GRCh38 human reference genome using STAR (version 2.7.2b)[35].
271 BAM files were ordered and indexed using Samtools[36]. Read counts on genes were
272 determined using StringTie[37]. Genes differentially expressed between conditions were
273 identified using the R package DESeq2 (version 1.34.0)[38]. Genes with an adjusted P-
274 value < 0.05 found by DESeq2 were assigned as differentially expressed. We assessed
275 the presence of desired *NFKB2* edits according to the CRISPR sgRNA design by direct
276 visualization of the BAM files and the absence of off-target coding variations by the
277 GATK Haplotype Caller GVCF tool[33].

278

279 **Total RNA isolation and quantitative real-time PCR (qRT-PCR) analysis for**
280 **assessment of mRNA expression of pituitary organoids development**

281 Organoids were harvested, placed on ice and stored dry at -80°C until RNA extraction.
282 The total RNA was extracted from WT, *TBX19*$^{K146R/K146R}$ and *NFKB2*$^{D865G/D865G}$ organoids
283 using the NucleoSpin RNA Plus XS kit (Macherey-Nagel), and measured on a NanoDrop
284 TM 1000 Spectrophotometer (Thermo Fisher Scientific). Organoid RNAs were extracted
285 on days 0, 6 and 18 from 7 or 8 organoids, or on days 27, 48, 75 and 105 from single
286 organoids (3-8 organoids per group for each time point). cDNA was synthesized from
287 200 ng total RNA using a mix of M-MLV reverse transcriptase (Invitrogen, UK,
288 #28025013), dNTP 10mM (Invitrogen, #10297018), RNAseOut Inhibitor (Invitrogen,
289 #10777019) and random primers (Invitrogen, UK, #48190011). Quantitative PCR was
290 performed using iTaq Universal SYBR Green Supermix (Bio-Rad Laboratories), on a
291 QuantStudio™ 5 Real-time PCR system (Thermo Fisher Scientific) and analysed using
292 QuantStudio™ 5 Design & Analysis Software. The thermal cycling profiles were as
293 follows: initial denaturation at 95°C for 20 seconds, followed by 40 cycles of
294 denaturation at 95°C (3 sec), annealing at 60°C (45 sec) and extension at 72°C (45 sec).
295 All samples were assayed in duplicate. The beta-actin (*ACTB*), glyceraldehyde-3-
296 phosphate dehydrogenase (*GAPDH*) and beta-tubulin (*TUBB)* transcripts expressions
297 were used as three endogenous reference controls. Target gene expressions were
298 normalized relative to the mean of the housekeeping genes using the delta Ct method,
299 and then normalized relative to the highest mean values of WT during the 105 days
300 using the comparative $2^{-\Delta\Delta Ct}$ method[39]. Primer sequences used in the experiments are
301 shown in **Suppl Table S7**.

302

303 **Immunofluorescence labeling experiments**

304 At days 48 and 105, ten each of WT and mutant organoids were fixed using 4% buffered
305 paraformaldehyde in standard phosphate-buffered saline (PBS) for an hour at RT before
306 rinsing in PBS. After overnight incubation in 30% sucrose/PBS (w/v) at 4°C, organoids
307 were embedded in Surgipath medium (Leica,# 3801480) and snap frozen. Organoids
308 were cryosectioned at 16 µm. After blocking with 0.01% Triton X100 (Sigma-Aldrich,
309 #329830772), 10% normal donkey serum (Millipore, USA, #S30-100 ML) and 1% fish
310 skin gelatin (Sigma-Aldrich, Canada, #G7765-250 ML) in PBS with 5 ng/mL 4',6-
311 diamidino-2-phénylindole (DAPI) for an hour at RT, slides were incubated with primary
312 antibody diluted in antibody solution (PBS, Triton as above, 1% normal donkey serum
313 and 0.1% fish skin gelatin) overnight at 4°C, washed and incubated and a 1/500 dilution
314 of secondary antibody in PBS for 2 hours at RT. The primary antibodies and dilutions
315 used in this study are summarized in **Suppl Table S8**. Secondary antibodies were
316 species-specific conjugates to Alexa Fluor 488, 555 or 647 (Thermo Fisher Scientific).
317 Fluorescence images were obtained using LSM 800 confocal microscopy (Zeiss).

318

319 **3D imaging of pituitary organoids**

320 We used a whole-mount immunostaining and clearing protocol adapted from Belle et al
321 [40]. 4-8 organoids of each genotype (WT, *TBX19*$^{K146R/K146R}$ or *NFKB2*$^{D865G/D865G}$) were fixed
322 by immersion in 4 % buffered paraformaldehyde (PFA) in PBS overnight at 4°C. All
323 steps were carried out on a slowly rotating (70 rpm) agitator. After washing in PBS,
324 organoids were either stored at 4°C or blocked and permeabilized with 5 mL PBSGT for
325 2 days at RT (PBSGT: 0.2% fish skin gelatin, 0.5% Triton X100 in PBS, NaN_3 0.01%).
326 Organoids were incubated with primary antibodies in 3 mL PBSGT (at concentrations
327 used on sections) over 5 days at 37°C to increase penetration. Organoids were then

328 washed 6 times in an excess of PBSGT at RT, before incubation with secondary
329 antibodies in 3 ml PBSGT at RT overnight. The wash step was repeated. Organoids were
330 then embedded in 1% low-melting temperature agarose in 1X TAE after it had cooled to
331 about 45°C.
332 As adapted from the iDISCO+ protocol[41], organoids in agarose blocks were
333 progressively dehydrated to 100% methanol (VWR, #20847.360) with 1h at each
334 graded step. After overnight incubation in two parts dichloromethane (DCM, Sigma-
335 Aldrich, #270997) to one part 100% methanol, organoids were immersed in 100% DCM
336 for 30 minutes before changing to 100% dibenzyl ether (DBE; Sigma-Aldrich, #108014)
337 for transparization over two hours. Samples were maintained in DBE at RT and
338 protected from light in an amber glass vial. Just before imaging, they were transferred to
339 room-temperature ethyl cinnamate (Sigma-Aldrich, #112372). Light-sheet fluorescence
340 microscopy (Miltenyi Biotec UltraMicroscope Blaze™) was used to acquire z-stacks of
341 optical sections of pituitary organoids at 4 μm intervals. After 3D reconstruction with
342 Imaris software (version 9.6, Bitplane), the number of corticotrophs in each organoid
343 was defined by counting individualized cell-sized (7 μm) objects positive for ACTH
344 immunoreactivity with the Spots automatic classifier after setting parameters in a
345 region of interest containing positively labeled WT cells, then applied to all organoids.
346 Using the Surfaces tool of the Imaris software, the volume of organoids was determined
347 separately, based on thresholds corresponding to their respective fluorescence
348 intensities.

349 **Statistical analysis**

350 Statistical analyses were performed and visualized with GraphPad Prism 9.5.0 software
351 (GraphPad Software, Inc). Data are expressed as means ± SEM. Comparisons between
352 the two groups (mutant versus WT) were performed by unpaired two-tailed t-tests
353 (non-parametric Mann-Whitney test). n refers to the number of samples for each

experiment outlined in the figure legends. p values of < 0.05 (*), < 0.01 (**), and < 0.001 (***) were considered statistically significant differences.

357 **Results**

358 **Corticotroph deficiency can be modeled by directed differentiation of *TBX19*-**
359 **mutant hiPSC in 3D culture**

360 To first validate the pituitary organoid model and determine whether the *TBX19* mutant
361 can affect corticotroph differentiation, we generated a homozygous *TBX19*$^{K146R/K146R}$
362 hiPSC line from the isogenic control line using CRISPR/Cas9 (**Figures 1A-1D; Suppl.**
363 **Figure S1**). One KI clone carrying *TBX19*$^{K146R/K146R}$ was obtained after screening 100
364 clones by CAPS and confirmed by Sanger sequencing (**Suppl Figure S2**). This mutant
365 clone was then amplified and differentiated into pituitary organoids, in parallel with the
366 control line.

367 The ability of the *TBX19*$^{K146R/K146R}$ line to differentiate into a hypothalamic-pituitary
368 structure was compared to its control line (200 organoids for each line) using a 3D
369 culture method, in which pituitary-like and hypothalamus-like tissues simultaneously
370 developed (**Figures 1E, 2A, Suppl Figure S3A-B**). Inside of such organoids, hiPSC
371 differentiate into hypothalamic progenitors, while the outer layer differentiates into an
372 epithelium sharing properties with the oral ectoderm that develops into Rathke's pouch
373 and then the anterior pituitary (**Figure 2A**, **Suppl Figure S3**). The expression of several
374 key markers of pituitary development and differentiation was followed in mutant
375 *TBX19*$^{K146R/K146R}$ organoids matched to control WT organoids over time, using qRT-PCR
376 (d0, d6, d18, d27, d48, d75, d105) and immunofluorescence (d48 and d105) (**Figure**
377 **2A)**. Organoids grew from 0.4 mm on day 6 to 1.9 mm in their largest 2D dimension by
378 day 105 (**Figure 2B**).

379 Successful differentiation was validated in WT organoids by qRT-PCR, at early stages
380 with the expression of a set of pituitary transcription factors, including *HESX1*, *PITX1*
381 and *LHX3*, and at the latest stage by the expression of corticotroph cell markers *TBX19*

382 and *POMC* (**Figures 2A, 2C-2G**). HESX1 is the first specific transcription factor of the
383 prospective pituitary and its expression is vital for the early determination of the gland.
384 In WT organoids, *HESX1* was expressed on day 6 and rapidly downregulated as of day
385 18 (**Figure 2C**). Expression of *PITX1* (a Rathke's pouch marker) and *LHX3* (a pituitary
386 progenitor marker) was high as of day 27, then reached stable levels from d48 onwards
387 (**Figures 2D-2E**). Importantly, immunofluorescence demonstrated effective generation
388 of pituitary progenitors in WT organoids with the appearance of LHX3+ cells in the oral
389 ectoderm-like epithelium by day 48 (**Figure 3A, Suppl Figure S3A**). This epithelium
390 also expressed PITX1 and E-cadherin (**Suppl Figure S3C**). Hypothalamus progenitors
391 expressed NKX2.1 (**Suppl Figure S3B**). By day 105, we observed that WT organoids
392 contained many differentiated corticotroph cells, co-expressing TBX19 protein in the
393 nucleus and ACTH in the cytoplasm as seen in confocal microscopy, a critical feature for
394 the rest of our investigations (n=8, **Figure 3B, Suppl Figure S3D**). Consistent with
395 these images, qRT-PCR results confirmed the highest levels of *TBX19* and *POMC*
396 transcription at day 105 in WT organoids (**Figures 2F-2G**). Taken together, these data
397 showed that pituitary organoids in 3D culture mimic important aspects of human
398 pituitary ontogenesis, and were characterized by the ability to differentiate into
399 pituitary progenitors by day 48 and then to corticotroph cells by day 105.

400 We then tested whether *TBX19*-mutant organoids could be used to model ACTHD. To
401 this end, pituitary organoids carrying $TBX19^{K146R/K146R}$ were cultured in parallel with
402 WT organoids and analyzed using qRT-PCR and immunofluorescence for the pituitary
403 ontogenesis markers as described above. Our data showed that there was no significant
404 difference in the expression of *HESX1* (**Figure 2C**). However, *PITX1* expression was
405 significantly decreased by days 48 (p= 0.0022) and 75 (p= 0.0159) in mutant organoids
406 (**Figure 2D**). There were significantly lower levels of *LHX3* expression (p= 0.004 on day
407 27, p= 0.0022 on day 48 and p= 0.0079 on day 75 (**Figure 2E**), although there was no

408 significant change in the expression of the *TBX19* transcript itself (p= 0.195 on day 75,
409 **Figure 2F**). Importantly, *POMC* expression was significantly decreased in the
410 *TBX19*$^{K146R/K146R}$ organoids by days 48 (p= 0.026), 75 (p= 0.0159) and 105 (p= 0.0317)
411 (**Figure 2G**).

412 Next, we checked several pituitary markers by immunofluorescence (**Figures 3A-3D**).
413 In line with the qRT-PCR results, *TBX19*$^{K146R/K146R}$ organoids immunostaining on day 48
414 showed that LHX3 protein expression was decreased, in contrast to WT organoids (n=
415 10 organoids for each group, **Figures 3A, 3C**). By day 105, we observed that there were
416 fewer corticotroph cells expressing ACTH and TBX19 protein in *TBX19*$^{K146R/K146R}$
417 organoids (n= 10 organoids for each group, **Figures 3B, 3D**).

418 Finally, in order to take into account the possibility of regionalized sampling or damage
419 in the process of histological section, we also confirmed that ACTH production was
420 nearly abolished in *TBX19*$^{K146R/K146R}$ organoids overall on day 105 as compared to
421 control organoids. To make this assessment, whole organoids were rendered
422 completely transparent using a previously validated clearing protocol and imaged by
423 light-sheet microscopy for quantitative analyses (**Figures 4A-4B** and **Suppl Movies 1-**
424 **2**). Indeed, differentiation into corticotroph cells was not uniform throughout the
425 organoids but was concentrated in one or multiple buds. These data demonstrate that
426 the *TBX19*$^{K146R/K146R}$ genotype leads to a significant decrease in ACTH+ corticotroph cell
427 numbers by day 105 as compared to control organoids (p= 0.0159, WT n=4, mutant
428 n=5, **Figure 4C**).

429 Together, this first set of experiments demonstrated that genome editing of hiPSC
430 bearing a homozygous pathogenic variant of *TBX19* prevented their differentiation into
431 ACTH-producing corticotrophs.
432

433 **NFKB2 signaling is vital for corticotroph development**

434 After validating this organoid model for the study of ACTHD with a known *TBX19*
435 missense mutation, we used the same approach to investigate the potential role of
436 NFKB2 during hypothalamic-pituitary development. The *NFKB2*^{D865G} homozygous
437 mutation was chosen because it was shown to severely affect NFKB2 p52 processing[12].
438 To do so, we first established a *NFKB2*$^{D865G/D865G}$ mutant hiPSC line using CRISPR/Cas9
439 (**Figure 5**) from the same isogenic control line. Two homozygous KI clones carrying
440 *NFKB2*$^{D865G/D865G}$ were obtained after screening by CAPS and confirmation by Sanger
441 sequencing (**Suppl Figure S4**). RNA-seq analyses confirmed the absence of mutation in
442 the top four predicted off-target sites. We then selected one homozygous missense
443 mutation *NFKB2*$^{D865G/D865G}$ clone (#7) to amplify and generate 200 mutant organoids in
444 parallel with 200 WT organoids in 3D culture.

445 Next, we compared the development and differentiation of the *NFKB2*$^{D865G/D865G}$ versus
446 WT organoids during culture by qRT-PCR and immunofluorescence as described above.
447 *HESX1* showed no significant difference in expression over time (**Figure 6A**). In
448 contrast, *PITX1* and *LHX3* were significantly decreased in *NFKB2*$^{D865G/D865G}$ organoids on
449 days 27 and 48 (**Figures 6B-6C**). Surprisingly, at the latest stage of differentiation (day
450 105), we observed a significant increase in *TBX19* expression in the mutant group (p=
451 0.0095, WT n=4, mutant n=6, **Figure 6D**). In contrast, *POMC* expression levels were
452 significantly lower in *NFKB2*$^{D865G/D865G}$ organoids compared to WT (p= 0.019, **Figure**
453 **6E**). Of note, as MRI has revealed pituitary hypoplasia in 43% of patients with DAVID
454 syndrome[42], we asked whether mutant organoids might be smaller than WT organoids.
455 However, after calculating the volume of organoids on day 105 using Imaris software,
456 these were not significantly different (p= 0.6, WT n=7, mutant n= 8, **Figure 6F**).
457 Concordant with qRT-PCR results, immunostaining showed less LHX3 expression in

458 *NFKB2*$^{D865G/D865G}$ organoids on day 48 compared to WT (**Figures 7A-7B**). Similar results
459 were obtained from ten individual organoids for each line. NFKB2 was co-expressed in
460 LHX3+ pituitary progenitors on day 48 (**Figure 7A**). Unexpectedly, NFKB2 was
461 markedly less expressed in *NFKB2*$^{D865G/D865G}$ organoids than in WT organoids (**Figures**
462 **7A-7B**). On day 105, immunostaining demonstrated fewer ACTH+ cells; in addition,
463 some TBX19+ cells expressed no simultaneous ACTH signal in *NFKB2*$^{D865G/D865G}$
464 organoids (**Figures 7C-7D)**.

465 Three-dimensional reconstruction of whole organoids highlighted this significantly
466 decreased ACTH expression in *NFKB2*$^{D865G/D865G}$ organoids on day 105 as compared to
467 WT in both qualitative (**Figures 8A-8B** and **Suppl Movies 3-4**) and quantitative
468 (p=0.0007, WT n=6, mutant n=8 **Figure 8C**) assessments. In the absence of an immune
469 system, this is strong evidence in support of a direct role for NFKB2 signaling in
470 pituitary differentiation.

471 To investigate downstream pathways altered in *NFKB2*$^{D865G/D865G}$ pituitary organoids,
472 we performed bulk RNA-seq of five distinct *NFKB2*$^{D865G/D865G}$ organoids versus five
473 organoids derived from its isogenic hiPSC control line on day 48. Differential expression
474 (DE) gene analysis identified 2,829 significantly upregulated and 2,586 significantly
475 downregulated genes at adjusted p (pAdj) < 0.05. The global results are depicted as a
476 heatmap to show the similarities across organoids sharing genotypes (**Figure 9A**) and a
477 volcano plot to highlight the magnitudes of DE between the two groups (**Figure 9B**).

478 Global NFKB signaling was not affected in *NFKB2*$^{D865G/D865G}$ organoids, as most genes
479 assigned to that pathway had fold-change values between -0.5 and 0.5, when they were
480 significant (**Suppl Figure S5**). However, among a list of 143 genes known to have a
481 functional influence on pituitary-hypothalamic development curated from the published
482 literature and also expressed in our model, 66 of these were found to be DE in

483 *NFKB2*$^{D865G/D865G}$ organoids (pAdj < 0.05; **Figure 9B, and Table 1**). 42 genes had
484 transcript level changes of two-fold or more and 21 of these were transcription factors
485 (**Figure 9C**). Expression of most of these transcription factors was downregulated, with
486 a marked decrease in expression of anterior pituitary progenitor markers such as *PITX1*
487 and *LHX3,* as well as lineage precursor markers *PROP1* and *POU1F1* (**Figure 9C and**
488 **Table 1)**. In contrast, the earliest Rathke's pouch marker, *HESX1,* showed a 2-fold
489 increased expression in *NFKB2*$^{D865G/D865G}$ organoids, suggesting an impaired progression
490 of pituitary progenitors towards more differentiated stages, with increased expression
491 of epithelial markers *CDH1*, *KRT8* and *CLDN6* and decreased transcription of
492 mesenchymal markers *CDH2* and *VIM* supporting that hypothesis (**Figure 9C and Table**
493 **1)**.

494 The transcription factor *RAX* also showed a moderate but significant decrease in its
495 expression (fold change = -0.6, padj < 0.05) in *NFKB2*$^{D865G/D865G}$ organoids (**Figure 9C**
496 **and Table 1)**, suggesting that the phenotype could be due, at least partially, to a
497 hypothalamic defect. Indeed, among the factors known to mediate the interaction
498 between the hypothalamus and oral ectoderm during pituitary development, *BMP4* and
499 *FGF10* had significant fold-changes of 4.35 and 0.26 in *NFKB2*$^{D865G/D865G}$ organoids
500 respectively, whereas *SHH*, *WNT5A* and *FGF8* expression levels were not modified
501 (**Table 1**). Finally, a 2.4-fold increase in *FST* expression, a gene recently identified as a
502 marker of differentiating corticotrophs[16], and concomitantly decreased levels of mature
503 corticotroph markers *AR*, *NR4A2*, *PCSK1* and *POMC* (0.63, 0.4, 0.35 and 0.43-fold
504 changes respectively) (**Table 1**), corroborate the hypothesis that TBX19-positive
505 precursors fail to achieve terminal differentiation in *NFKB2*$^{D865G/D865G}$ organoids.

506 Taken together, our data identify NFKB2-mediated signaling as an important factor
507 acting on pituitary development at multiple levels during its maturation.
508

509 **Discussion**

510 After describing the rare combination of an anterior pituitary deficit, mostly ACTHD,
511 with common variable immunodeficiency in DAVID syndrome, we and others found that
512 affected patients carry *NFKB2* gene mutations affecting specific C-terminal residues of
513 the NFKB2 protein known to play important roles in immunity [7,8,9]. As the spontaneous
514 mouse knockout mutant of the orthologous gene lacks an endocrine phenotype, yet
515 *NFKB2* is transcribed in the prenatal human pituitary gland, we wanted to investigate
516 the mechanisms of ACTHD in a human disease model.

517 The available *in vitro* models to study ACTHD and CPHD had strong limitations. For
518 instance, studies based on transfections and luciferase-coupled hormone promoters can
519 only give indirect evidence of the effect of a variant of unknown significance on the
520 activity of a given transcription factor, as they are based on non-physiological amounts
521 of DNA and promoter constructs[5]. Murine models only partially replicate human CPHD,
522 as already shown for *PROP1* mutations in ACTHD (absent in mice but present in 40% of
523 humans)[43]. However, reprogramming differentiated adult cells into induced pluripotent
524 stem cells and advances in genome editing technologies using CRISPR/Cas9 broadened
525 possibilities for modeling novel aspects of human disease *ex vivo*[44]. Organoid culture has
526 allowed the modeling of otherwise inaccessible congenital human disorders affecting
527 the brain[25], intestine[45], kidney[46], liver[47], pancreas[48], ovary[49], and lung[50]. In the present
528 study, we established a human *in vitro* model of congenital ACTHD using 3D pituitary
529 organoids differentiated from $TBX19^{K146R/K146R}$ and $NFKB2^{D865G/D865G}$ hiPSC generated by
530 CRISPR/Cas9 genome editing, in order to compare them with their isogenic WT
531 equivalents. After confirming that this model could recapitulate relevant aspects of
532 pituitary development, we then determined whether it could also replicate a disease,
533 namely ACTHD.

534 As the *TBX19*^{K146R} homozygous variant is known to cause ACTHD in humans, we
535 designed a human organoid model derived from *TBX19*$^{K146R/K146R}$ hiPSC as a proof of
536 principle. In line with the *Tbx19*$^{-/-}$ mouse model[3], *TBX19*$^{K146R/K146R}$ organoids displayed
537 markedly defective corticotroph differentiation, as compared to WT organoids, thereby
538 validating the methodological approach. Interestingly, in organoids carrying a
539 *TBX19*$^{K146R/K146R}$ missense mutation that affects DNA binding, a few corticotroph cells
540 were still present, suggesting either a role for TBX19 independent of its DNA binding
541 activity or persistence of residual DNA binding activity with this mutation.

542 Using this same approach with *NFKB2*$^{D865G/D865G}$ organoids generated by CRISPR/Cas9-
543 edited hiPSC, we demonstrated for the first time a role for NFKB2 in pituitary
544 development. Heterozygous mutations in the C-terminal region of *NFKB2*, such as
545 D865G, were reported in DAVID syndrome, leading to the disruption of both non-
546 canonical and canonical pathways[8,11–13,51,52]. Although *NFKB2*^{D865G} has been identified in
547 a heterozygous state in patients with ACTHD, we decided to generate a homozygous
548 model of *NFKB2*$^{D865G/D865G}$ to determine first whether NFKB2 was involved in human
549 pituitary development at all and could explain the defect in ACTH production in DAVID
550 syndrome (OMIM#, 615577) [7,8,53]. Indeed, while concomitant common variable immune
551 deficiency (CVID) can be explained by the key roles of NFKB signaling in the immune
552 system, the mechanism of the endocrine deficits caused by *NFKB2* mutations was
553 unknown. In mouse models, deletion of *Nfkb2* causes abnormal germinal center B-cell
554 formation and differentiation[14]. However, the spontaneous *Lym1* mouse model, which
555 carries a truncating variant Y868* in the *Nfkb2* orthologue that prevents its cleavage
556 into a transcriptionally active form, had apparently normal corticotroph function and
557 ACTH expression in the pituitary in both heterozygotes and homozygotes[9]. Mutant
558 *Nfkb2* homozygotes do display reduced fertility and more severe immune abnormalities
559 than their heterozygous counterparts [54]. Using pituitary organoids differentiated from a

560 *NFKB2*$^{D865G/D865G}$ hiPSC line in comparison with its unmutated control and in the absence
561 of an immune response, we have demonstrated that human corticotroph development
562 is directly disrupted by the same missense mutation found in DAVID syndrome.

563 The precise molecular mechanisms by which NFKB2 impairs corticotroph development
564 remain to be determined. However, our results suggest both early and late effects on
565 corticotroph differentiation. First, NFKB2 may be involved in the early steps of pituitary
566 development. RNA-seq data on day 48 of *NFKB2*$^{D865G/D865G}$ organoid development
567 showed increased *HESX1* and *BMP4* transcription, which may reflect blockade in an
568 undifferentiated state evocative of the Rathke's pouch epithelial primordium: indeed,
569 down-regulation of HESX1 is necessary for proper pituitary development[55]. This is also
570 supported by RNA-seq results showing downregulation of *PITX1, HES1, LHX3* and *FGF10*
571 in mutant organoids, as their expression is known to be necessary for progression to a
572 later progenitor state[56,57]. Finally, concordant with the hypothesis of a differentiation
573 blockade, upregulation of epithelial markers such as E-cadherin and keratin-8 was
574 observed in mutant *NFKB2*$^{D865G/D865G}$ organoids on day 48 while in contrast, there were
575 no changes in Wnt and hedgehog signaling pathways. Second, NFKB2 could also be
576 involved in the final steps of corticotroph differentiation. While qRT-PCR showed
577 increased levels of *TBX19* mRNA in mutant organoids, this did not lead to the expected
578 increase in *POMC* mRNA transcripts. Similarly, some *NFKB2* mutants had TBX19+ cells
579 without simultaneous ACTH expression. This suggests that NFKB2 is necessary for
580 POMC synthesis in TBX19-specified cells, which *NFKB2*^{D865G} may prevent. This could be
581 due to abnormal DNA binding of the NFKB heterodimer to the *POMC* promoter[58,59]
582 and/or regulation of *PCSK1*, the gene coding for the enzyme necessary to convert POMC
583 to ACTH. Alternatively, *NFKB2*^{D865G} could also block TBX19+ cells in a pre-differentiated
584 corticotroph state through its derepression of chromatin remodeling factors such as
585 EZH2[60].

586 The organoid model described in this paper presents several advantages over other
587 approaches. It is a true human model of ACTHD, emphasizing the limits of mouse
588 models as exemplified by the *Lym1* model, which showed that Nfkb2 was dispensable
589 for murine pituitary development. Despite some technical constraints, CRISPR/Cas9-
590 based genome editing of hiPSC is a powerful approach to elucidate gene function in
591 congenital pituitary deficiency patients, as shown for the role of hypothalamic OTX2
592 regulation of pituitary progenitor cells in congenital pituitary hypoplasia[20]. While the
593 prevalence of pathogenic variants of known genes in primary hypopituitarism is
594 currently estimated to be below 10%[6], exome and whole-genome sequencing regularly
595 identify new genes and variants, for which pathogenicity remains uncertain[35]. This
596 model or refinements thereof could thus become the gold standard to confirm
597 involvement of a given gene in human anterior pituitary development, or to classify new
598 variants of unknown significance as likely benign or pathogenic. Finally, pituitary
599 organoids derived from human embryonic stem cells have been transplanted
600 subcutaneously into mice with hypopituitarism; grafted cells were able to secrete ACTH
601 and respond to corticotropin-releasing hormone stimulation[61]. The near future may
602 therefore promise patients with hypopituitarism innovative substitutive treatments
603 with their own reprogrammed cells.

604 In conclusion, we have designed and validated a model replicating human constitutive
605 ACTHD using a combination of CRISPR/Cas9 and directed differentiation of hiPSC into
606 3D hypothalamic-pituitary organoids. Not only has this proof-of-concept reproduced
607 the known prerequisite for the TBX19 transcription factor in human corticotroph
608 differentiation, it has also allowed a new classification of a *NFKB2* variant of previously
609 unknown clinical significance as pathogenic in pituitary development. From a clinical
610 viewpoint, our organoid model can provide evidence for the pathogenic role of new
611 candidate genes or variants investigated in patients where none other is available,

612 especially in a rare disease affecting a poorly accessible organ like the pituitary gland.
613 From a physiological viewpoint, modeling corticotroph deficiency using hiPSC allows to
614 support the functional role of NFKB2 in human pituitary differentiation.

615

616

617

618 **Acknowledgments**

619 This study was supported by the ADEREM (Association pour le Développement de la
620 Recherche Médicale au CHU de Marseille), the Association Française contre les
621 Myopathies (AFM-Téléthon) MoThARD program and by Pfizer. TTM received funding
622 from France Excellence Scholarship of the French Embassy in Vietnam, from the French
623 Society of Pediatric Endocrinology and Diabetology (SFEDP) and from the Marseille
624 Rare Disease (MarMaRa) Institute of Aix-Marseille University. The authors wish to
625 thank Frederique Magdinier, Natacha Broucqsault and Claire El Yazidi from the
626 Marseille Medical Genetics (MMG) cell reprogramming & differentiation facility (MaSC);
627 Sébastien Courrier, from the MMG microscopy platform; Valerie Delague, Catherine
628 Aubert, Christel Castro and Camille Humbert from MMG's Genomics and Bioinformatics
629 (GBiM) platform; Carole Siret and Mathieu Fallet from the Centre d'Immunologie de
630 Marseille-Luminy (CIML); Ivo Vanzetta and Alberto Lombardini from the Institut de
631 Neurosciences de la Timone (INT) microscopy platform, and Laurie Arnaud and
632 Emmanuel Nivet from the Institut de Neurophysiopathologie (INP), all in Marseille, for
633 their expert assistance, advice or reagents.

634 **Declaration of interests**

635 The authors declare no competing interests.

636

References

1. Couture C, Saveanu A, Barlier A, et al. Phenotypic Homogeneity and Genotypic Variability in a Large Series of Congenital Isolated ACTH-Deficiency Patients with *TPIT* Gene Mutations. *The Journal of Clinical Endocrinology & Metabolism*. 2012;97(3):E486-E495. doi:10.1210/jc.2011-1659
2. Lamolet B, Pulichino AM, Lamonerie T, et al. A Pituitary Cell-Restricted T Box Factor, Tpit, Activates POMC Transcription in Cooperation with Pitx Homeoproteins. *Cell*. 2001;104(6):849-859. doi:10.1016/S0092-8674(01)00282-3
3. Pulichino AM, Vallette-Kasic S, Couture C, et al. Human and mouse *TPIT* gene mutations cause early onset pituitary ACTH deficiency. *Genes Dev*. 2003;17(6):711-716. doi:10.1101/gad.1065603
4. Reynaud R, Gueydan M, Saveanu A, et al. Genetic screening of combined pituitary hormone deficiency: experience in 195 patients. *J Clin Endocrinol Metab*. 2006;91(9):3329-3336. doi:10.1210/jc.2005-2173
5. Jullien N, Romanet P, Philippon M, et al. Heterozygous LHX3 mutations may lead to a mild phenotype of combined pituitary hormone deficiency. *Eur J Hum Genet*. 2019;27(2):216-225. doi:10.1038/s41431-018-0264-6
6. Jullien N, Saveanu A, Vergier J, et al. Clinical lessons learned in constitutional hypopituitarism from two decades of experience in a large international cohort. *Clin Endocrinol (Oxf)*. 2021;94(2):277-289. doi:10.1111/cen.14355
7. Quentien MH, Delemer B, Papadimitriou DT, et al. Deficit in Anterior Pituitary Function and Variable Immune Deficiency (DAVID) in Children Presenting with Adrenocorticotropin Deficiency and Severe Infections. *The Journal of Clinical Endocrinology & Metabolism*. 2012;97(1):E121-E128. doi:10.1210/jc.2011-0407
8. Chen K, Coonrod EM, Kumánovics A, et al. Germline Mutations in NFKB2 Implicate the Noncanonical NF-κB Pathway in the Pathogenesis of Common Variable Immunodeficiency. *The American Journal of Human Genetics*. 2013;93(5):812-824. doi:10.1016/j.ajhg.2013.09.009
9. Brue T, Quentien MH, Khetchoumian K, et al. Mutations in NFKB2 and potential genetic heterogeneity in patients with DAVID syndrome, having variable endocrine and immune deficiencies. *BMC Med Genet*. 2014;15:139. doi:10.1186/s12881-014-0139-9
10. Wirasinha RC, Davies AR, Srivastava M, et al. *Nfkb2* variants reveal a p100-degradation threshold that defines autoimmune susceptibility. *Journal of Experimental Medicine*. 2021;218(2):e20200476. doi:10.1084/jem.20200476
11. Kuehn HS, Niemela JE, Sreedhara K, et al. Novel nonsense gain-of-function NFKB2 mutations associated with a combined immunodeficiency phenotype. *Blood*. 2017;130(13):1553-1564. doi:10.1182/blood-2017-05-782177
12. Lee CE, Fulcher DA, Whittle B, et al. Autosomal-dominant B-cell deficiency with alopecia due to a mutation in NFKB2 that results in nonprocessable p100. *Blood*. 2014;124(19):2964-2972. doi:10.1182/blood-2014-06-578542
13. Lindsley AW, Qian Y, Valencia CA, Shah K, Zhang K, Assa'ad A. Combined immune deficiency in a patient with a novel NFKB2 mutation. *J Clin Immunol*. 2014;34(8):910-915. doi:10.1007/s10875-014-0095-3
14. Carragher D, Johal R, Button A, et al. A Stroma-Derived Defect in NF-κB2−/− Mice Causes Impaired Lymph Node Development and Lymphocyte Recruitment. *The Journal of Immunology*. 2004;173(4):2271-2279. doi:10.4049/jimmunol.173.4.2271
15. Mac TT, Castinetti F, Bar C, et al. Deficient anterior pituitary with common variable immune deficiency (DAVID syndrome): a new case and literature reports. *J Neuroendocrinol*. Published online May 6, 2023:e13287. doi:10.1111/jne.13287
16. Zhang S, Cui Y, Ma X, et al. Single-cell transcriptomics identifies divergent developmental lineage trajectories during human pituitary development. *Nat Commun*. 2020;11(1):5275. doi:10.1038/s41467-020-19012-4

17. Ho BX, Pek NMQ, Soh BS. Disease Modeling Using 3D Organoids Derived from Human Induced Pluripotent Stem Cells. *Int J Mol Sci*. 2018;19(4):E936. doi:10.3390/ijms19040936
18. Ozone C, Suga H, Eiraku M, et al. Functional anterior pituitary generated in self-organizing culture of human embryonic stem cells. *Nat Commun*. 2016;7(1):10351. doi:10.1038/ncomms10351
19. Kasai T, Suga H, Sakakibara M, et al. Hypothalamic Contribution to Pituitary Functions Is Recapitulated In Vitro Using 3D-Cultured Human iPS Cells. *Cell Reports*. 2020;30(1):18-24.e5. doi:10.1016/j.celrep.2019.12.009
20. Matsumoto R, Suga H, Aoi T, et al. Congenital pituitary hypoplasia model demonstrates hypothalamic OTX2 regulation of pituitary progenitor cells. *Journal of Clinical Investigation*. 2019;130(2):641-654. doi:10.1172/JCI127378
21. Suga H, Kadoshima T, Minaguchi M, et al. Self-formation of functional adenohypophysis in three-dimensional culture. *Nature*. 2011;480(7375):57-62. doi:10.1038/nature10637
22. Sasai Y, Eiraku M, Suga H. In vitro organogenesis in three dimensions: self-organising stem cells. *Development*. 2012;139(22):4111-4121. doi:10.1242/dev.079590
23. Sun Y, Ding Q. Genome engineering of stem cell organoids for disease modeling. *Protein Cell*. 2017;8(5):315-327. doi:10.1007/s13238-016-0368-0
24. Giobbe GG, Michielin F, Luni C, et al. Functional differentiation of human pluripotent stem cells on a chip. *Nat Methods*. 2015;12(7):637-640. doi:10.1038/nmeth.3411
25. Arnaud L, Benech P, Greetham L, et al. APOE4 drives inflammation in human astrocytes via TAGLN3 repression and NF-κB activation. *Cell Rep*. 2022;40(7):111200. doi:10.1016/j.celrep.2022.111200
26. Ran FA, Hsu PD, Wright J, Agarwala V, Scott DA, Zhang F. Genome engineering using the CRISPR-Cas9 system. *Nat Protoc*. 2013;8(11):2281-2308. doi:10.1038/nprot.2013.143
27. Concordet JP, Haeussler M. CRISPOR: intuitive guide selection for CRISPR/Cas9 genome editing experiments and screens. *Nucleic Acids Res*. 2018;46(Web Server issue):W242-W245. doi:10.1093/nar/gky354
28. Paquet D, Kwart D, Chen A, et al. Efficient introduction of specific homozygous and heterozygous mutations using CRISPR/Cas9. *Nature*. 2016;533(7601):125-129. doi:10.1038/nature17664
29. Edmondson C, Zhou Q, Liu X. Analysis of conventional and alternative CRISPR/Cas9 genome editing to enhance a single-base pair knock-in mutation. *BMC Biotechnology*. 2021;21(1):45. doi:10.1186/s12896-021-00707-5
30. Kwart D, Paquet D, Teo S, Tessier-Lavigne M. Precise and efficient scarless genome editing in stem cells using CORRECT. *Nat Protoc*. 2017;12(2):329-354. doi:10.1038/nprot.2016.171
31. Zischewski J, Fischer R, Bortesi L. Detection of on-target and off-target mutations generated by CRISPR/Cas9 and other sequence-specific nucleases. *Biotechnology Advances*. 2017;35(1):95-104. doi:10.1016/j.biotechadv.2016.12.003
32. Li H, Durbin R. Fast and accurate short read alignment with Burrows–Wheeler transform. *Bioinformatics*. 2009;25(14):1754-1760. doi:10.1093/bioinformatics/btp324
33. Poplin R, Ruano-Rubio V, DePristo MA, et al. Scaling accurate genetic variant discovery to tens of thousands of samples. Published online July 24, 2018:201178. doi:10.1101/201178
34. McLaren W, Gil L, Hunt SE, et al. The Ensembl Variant Effect Predictor. *Genome Biology*. 2016;17(1):122. doi:10.1186/s13059-016-0974-4
35. Dobin A, Davis CA, Schlesinger F, et al. STAR: ultrafast universal RNA-seq aligner. *Bioinformatics*. 2013;29(1):15-21. doi:10.1093/bioinformatics/bts635
36. Twelve years of SAMtools and BCFtools | GigaScience | Oxford Academic. Accessed May 25, 2023. https://academic-oup-

742 com.proxy.insermbiblio.inist.fr/gigascience/article/10/2/giab008/6137722
743 37. Pertea M, Pertea GM, Antonescu CM, Chang TC, Mendell JT, Salzberg SL. StringTie
744 enables improved reconstruction of a transcriptome from RNA-seq reads. *Nat Biotechnol*.
745 2015;33(3):290-295. doi:10.1038/nbt.3122
746 38. Love MI, Huber W, Anders S. Moderated estimation of fold change and dispersion for
747 RNA-seq data with DESeq2. *Genome Biology*. 2014;15(12):550. doi:10.1186/s13059-014-
748 0550-8
749 39. Livak KJ, Schmittgen TD. Analysis of relative gene expression data using real-time
750 quantitative PCR and the 2(-Delta Delta C(T)) Method. *Methods*. 2001;25(4):402-408.
751 doi:10.1006/meth.2001.1262
752 40. Belle M, Godefroy D, Couly G, et al. Tridimensional Visualization and Analysis of
753 Early Human Development. *Cell*. 2017;169(1):161-173.e12. doi:10.1016/j.cell.2017.03.008
754 41. Renier N, Adams EL, Kirst C, et al. Mapping of brain activity by automated volume
755 analysis of immediate early genes. *Cell*. 2016;165(7):1789-1802.
756 doi:10.1016/j.cell.2016.05.007
757 42. Mac TT, Castinetti F, Bar C, et al. Anterior pituitary hormone deficiency in DAVID
758 syndrome. *Journal of Neuroendocrinology*. n/a(n/a):e13287. doi:10.1111/jne.13287
759 43. Castinetti F, Reynaud R, Saveanu A, et al. MECHANISMS IN ENDOCRINOLOGY:
760 An update in the genetic aetiologies of combined pituitary hormone deficiency. *European*
761 *Journal of Endocrinology*. 2016;174(6):R239-R247. doi:10.1530/EJE-15-1095
762 44. Randolph LN, Jiang Y, Lian X, Randolph LN, Jiang Y, Lian X. Stem Cell
763 Engineering and Differentiation for Disease Modeling and Cell-based Therapies. *CTE*.
764 2017;1(2):140-157. doi:10.3934/celltissue.2017.2.140
765 45. Schwank G, Koo BK, Sasselli V, et al. Functional repair of CFTR by CRISPR/Cas9
766 in intestinal stem cell organoids of cystic fibrosis patients. *Cell Stem Cell*. 2013;13(6):653-
767 658. doi:10.1016/j.stem.2013.11.002
768 46. Takasato M, Er PX, Chiu HS, et al. Kidney organoids from human iPS cells contain
769 multiple lineages and model human nephrogenesis. *Nature*. 2015;526(7574):564-568.
770 doi:10.1038/nature15695
771 47. Guan Y, Xu D, Garfin PM, et al. Human hepatic organoids for the analysis of human
772 genetic diseases. *JCI Insight*. 2017;2(17):e94954, 94954. doi:10.1172/jci.insight.94954
773 48. Moreira L, Bakir B, Chatterji P, Dantes Z, Reichert M, Rustgi AK. Pancreas 3D
774 Organoids: Current and Future Aspects as a Research Platform for Personalized Medicine in
775 Pancreatic Cancer. *Cellular and Molecular Gastroenterology and Hepatology*.
776 2018;5(3):289-298. doi:10.1016/j.jcmgh.2017.12.004
777 49. Nanki Y, Chiyoda T, Hirasawa A, et al. Patient-derived ovarian cancer organoids
778 capture the genomic profiles of primary tumours applicable for drug sensitivity and resistance
779 testing. *Sci Rep*. 2020;10(1):12581. doi:10.1038/s41598-020-69488-9
780 50. Kong J, Wen S, Cao W, et al. Lung organoids, useful tools for investigating epithelial
781 repair after lung injury. *Stem Cell Research & Therapy*. 2021;12(1):95. doi:10.1186/s13287-
782 021-02172-5
783 51. Liu Y, Hanson S, Gurugama P, Jones A, Clark B, Ibrahim MAA. Novel NFKB2
784 Mutation in Early-Onset CVID. *J Clin Immunol*. 2014;34(6):686-690. doi:10.1007/s10875-
785 014-0064-x
786 52. Maccari ME, Scarselli A, Di Cesare S, et al. Severe Toxoplasma gondii infection in a
787 member of a NFKB2-deficient family with T and B cell dysfunction. *Clinical Immunology*.
788 2017;183:273-277. doi:10.1016/j.clim.2017.09.011
789 53. Mac TT, Castinetti F, Bar C, et al. Anterior pituitary hormone deficiency in DAVID
790 syndrome. *Journal of Neuroendocrinology*. 2023.
791 54. Tucker E, O'Donnell K, Fuchsberger M, et al. A novel mutation in the Nfkb2 gene
792 generates an NF-kappa B2 "super repressor." *J Immunol*. 2007;179(11):7514-7522.
793 doi:10.4049/jimmunol.179.11.7514
794 55. Cohen RN, Cohen LE, Botero D, et al. Enhanced Repression by HESX1 as a Cause of

795 Hypopituitarism and Septooptic Dysplasia. *The Journal of Clinical Endocrinology &*
796 *Metabolism*. 2003;88(10):4832-4839. doi:10.1210/jc.2002-021868
797 56. Ohuchi H, Hori Y, Yamasaki M, et al. FGF10 acts as a major ligand for FGF receptor
798 2 IIIb in mouse multi-organ development. *Biochem Biophys Res Commun*. 2000;277(3):643-
799 649. doi:10.1006/bbrc.2000.3721
800 57. Ericson J, Norlin S, Jessell TM, Edlund T. Integrated FGF and BMP signaling
801 controls the progression of progenitor cell differentiation and the emergence of pattern in the
802 embryonic anterior pituitary. *Development*. 1998;125(6):1005-1015.
803 doi:10.1242/dev.125.6.1005
804 58. Giraldi FP, Cassarino F, Pagliardini L, Asnaghi V, Cavagnini F. The human POMC
805 gene promoter: Where do we stand? *J Endocrinol Invest*. 2011;34(6):454-460.
806 doi:10.1007/BF03346713
807 59. Drouin J. 60 YEARS OF POMC: Transcriptional and epigenetic regulation of POMC
808 gene expression. *Journal of Molecular Endocrinology*. 2016;56(4):T99-T112.
809 doi:10.1530/JME-15-0289
810 60. De Donatis GM, Le Pape E, Pierron A, et al. NF-kB2 induces senescence bypass in
811 melanoma via a direct transcriptional activation of EZH2. *Oncogene*. 2016;35(21):2735-
812 2745. doi:10.1038/onc.2015.331
813 61. Sasaki H, Suga H, Takeuchi K, et al. Subcutaneous transplantation of human
814 embryonic stem cells-derived pituitary organoids. *Frontiers in Endocrinology*. 2023;14.
815 Accessed April 12, 2023. https://www.frontiersin.org/articles/10.3389/fendo.2023.1130465

816

A *TBX19* gene

TBX19^{K146R} (AaG > AgG)

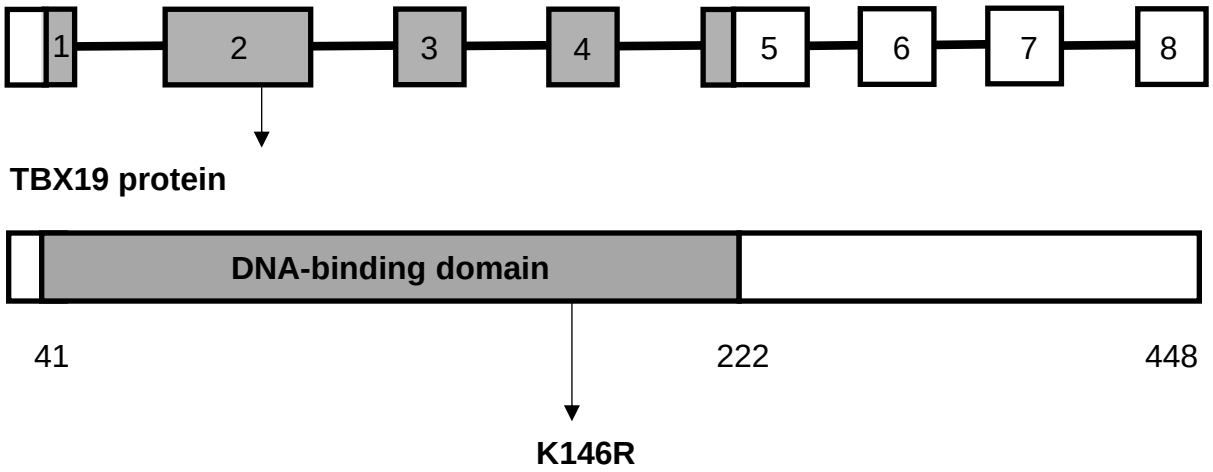

B WT

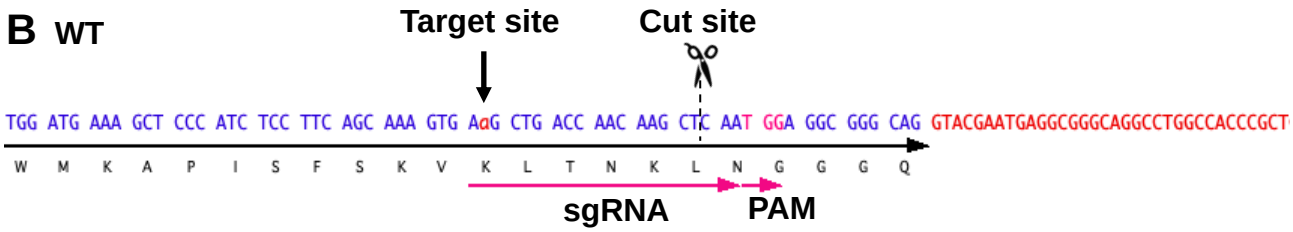

C ssODN

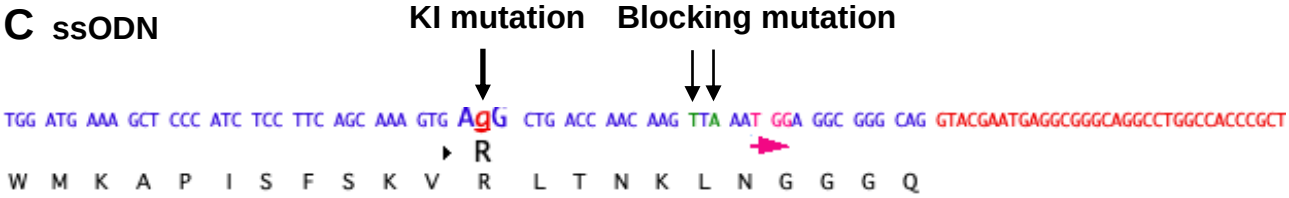

D

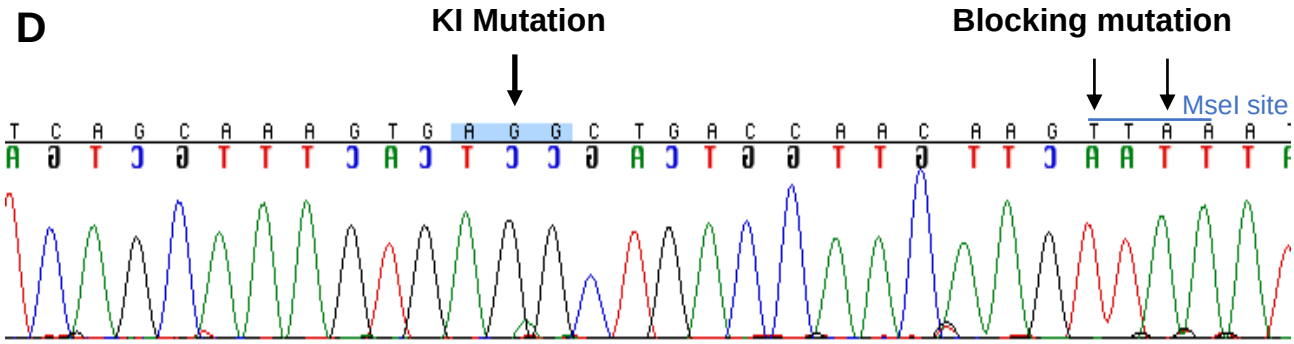

E

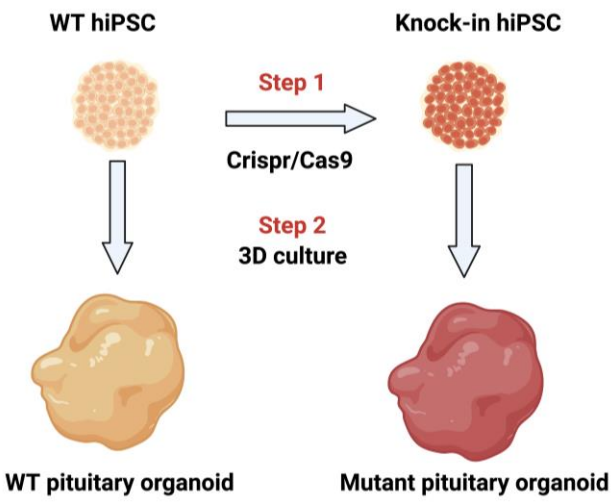

Figure 1: Design of sgRNA and ssODN to edit *TBX19*^{K146R} mutation

A, Illustration of the *TBX19* gene (HGNC: 11596; NCBI: NG_008244.1; Ensembl: ENSG00000143178; Human GRCh38) and TBX19 protein.

B, Wild-type (WT) sequence containing target site, cut site, target and PAM sequences.

C, ssODN design to edit in a missense K146R mutant of *TBX19* using CRISPR/Cas9.

D, Sequence analysis of a *TBX19*$^{K146R/K146R}$ hiPSC clone 63 obtained by Sanger sequencing after screening by CAPS. This clone was subsequently used in this work to differentiate into pituitary organoids (see below).

E, Summary of our strategy procedure:

Step 1: Production of the knock-in hiPSC lines by CRISPR/Cas9 genome editing.

Step 2: Differentiation into the pituitary organoids from mutant hiPSC lines in parallel with WT line using 3D culture, then comparison of the development of organoids between the two groups.

CAPS: cleaved amplified polymorphic sequences; hiPSC: human induced pluripotent stem cells; KI: knock-in; PAM: protospacer-adjacent motif; sgRNA: single guide RNA; ssODN: single-stranded oligo DNA nucleotides; WT: wildtype; 3D: three dimensions.

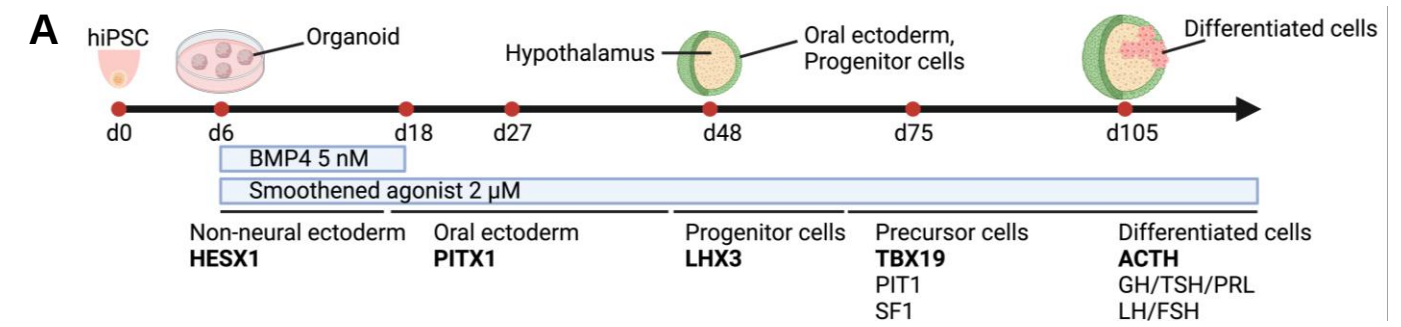
A
hiPSC
Organoid
Hypothalamus
Oral ectoderm,
Progenitor cells
Differentiated cells
d0
d6
d18
d27
d48
d75
d105
BMP4 5 nM
Smoothened agonist 2 μM
Non-neural ectoderm
HESX1
Oral ectoderm
PITX1
Progenitor cells
LHX3
Precursor cells
TBX19
PIT1
SF1
Differentiated cells
ACTH
GH/TSH/PRL
LH/FSH

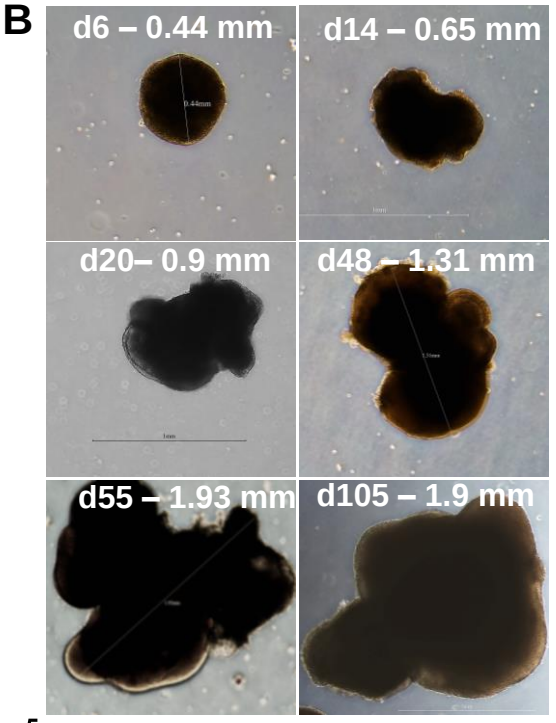
B
d6 – 0.44 mm
d14 – 0.65 mm
d20– 0.9 mm
d48 – 1.31 mm
d55 – 1.93 mm
d105 – 1.9 mm

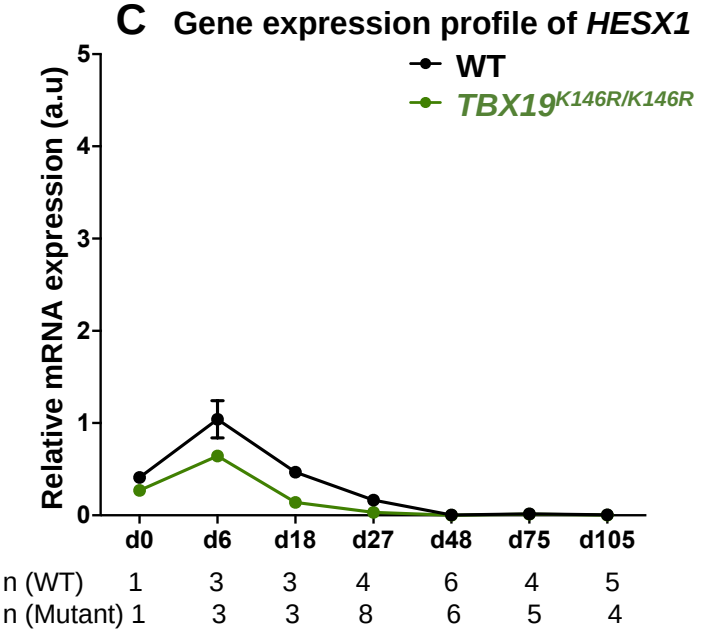
C Gene expression profile of HESX1
WT
TBX19K146R/K146R
Relative mRNA expression (a.u)
d0 d6 d18 d27 d48 d75 d105
n (WT) 1 3 3 4 6 4 5
n (Mutant) 1 3 3 8 6 5 4

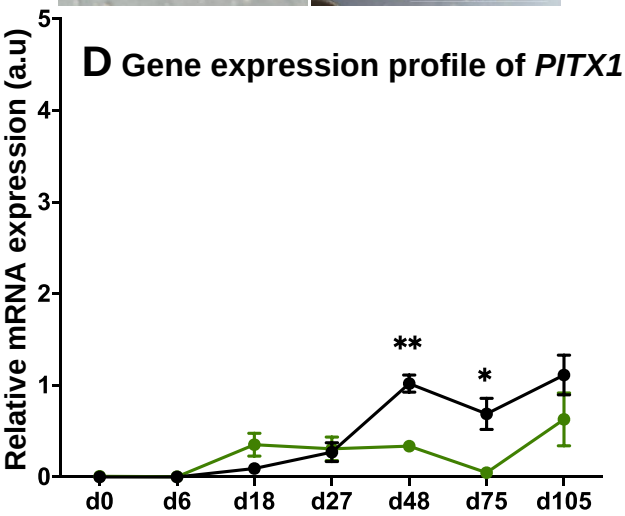
D Gene expression profile of PITX1
Relative mRNA expression (a.u)
**
*
d0 d6 d18 d27 d48 d75 d105

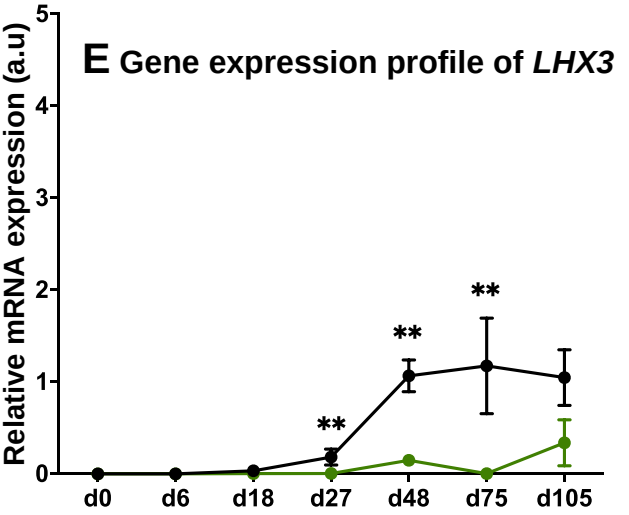
E Gene expression profile of LHX3
Relative mRNA expression (a.u)
**
**
**
d0 d6 d18 d27 d48 d75 d105

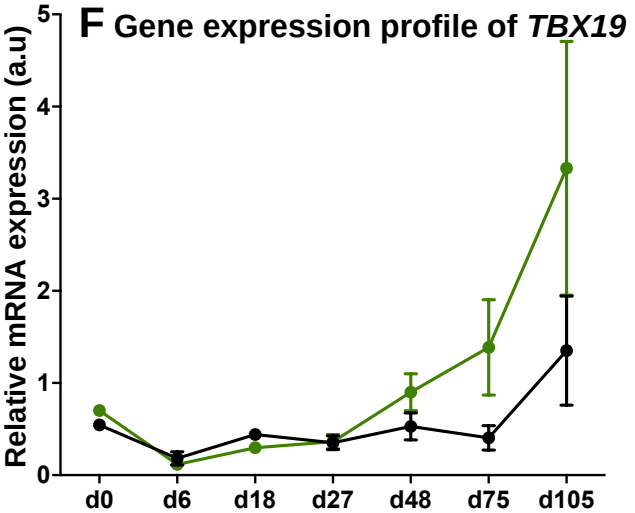
F Gene expression profile of TBX19
Relative mRNA expression (a.u)
d0 d6 d18 d27 d48 d75 d105

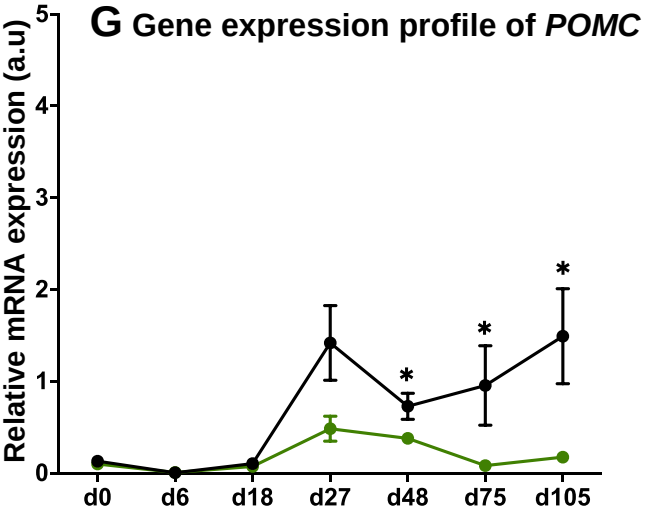
G Gene expression profile of POMC
Relative mRNA expression (a.u)
*
*
*
d0 d6 d18 d27 d48 d75 d105

Figure 2: **Time course of organoid growth and gene expression in WT and *TBX19*$^{K146R/K146R}$ organoids**

A, Culture protocol and schematic to generate pituitary organoids in three-dimensional (3D) culture from hiPSC. Organoids were collected at days (d) 0, 6, 18, 27, 48, 75, and 105 during differentiation to analyze.

B, Bright-field microscopy views of WT organoid examples at different time points throughout differentiation. Scale bars are indicated in each image.

C-G, Relative quantification (RQ) mRNA expression analysis for key markers of pituitary organoids during differentiation: WT (in black line) and *TBX19*$^{K146R/K146R}$ organoids (in green line). Data show means ± standard error of the mean (SEM); n=1 on day (d)0, n=3 samples per group (8 organoids per sample) at the time points d6 and d18, n=4-8 organoids per group at each subsequent time point (d27, d48, d75 and d105). Mann-Whitney t-test (unpaired, two-tailed, nonparametric). $p < 0.05$ (*), $p< 0.01$ (**).

C, Relative quantification expression of *HESX1*, one of the earliest pituitary placode markers. The expression of *HESX1* was not significantly different in *TBX19*$^{K146R/K146R}$ organoids vs. WT.

D, Relative quantification expression of *PITX1*, an anterior pituitary progenitor marker in the ectodermal primordium. *PITX1* was significantly downregulated in *TBX19*$^{K146R/K146R}$ organoids by d48 (** p= 0.0022) and d75 (* p= 0.0159).

E, Relative quantification expression of *LHX3*, a pituitary progenitor transcription factor. *LHX3* was significantly lower in *TBX19*$^{K146R/K146R}$ organoids as compared to WT on d27 (** p= 0.004), d48 (** p= 0.0022) and d75 (** p=0.0079).

F, Relative quantification expression of *TBX19*, a corticotroph lineage marker. There was no significant difference in *TBX19* expression between the two groups (p= 0.195, d75).

G, Relative quantification expression of *POMC*, a differentiated corticotroph marker. *POMC* was significantly downregulated in *TBX19*$^{K146R/K146R}$ organoids by d48 (* p= 0.026) and thereafter (* p= 0.0159 on d75; * p= 0.0317 on d105).

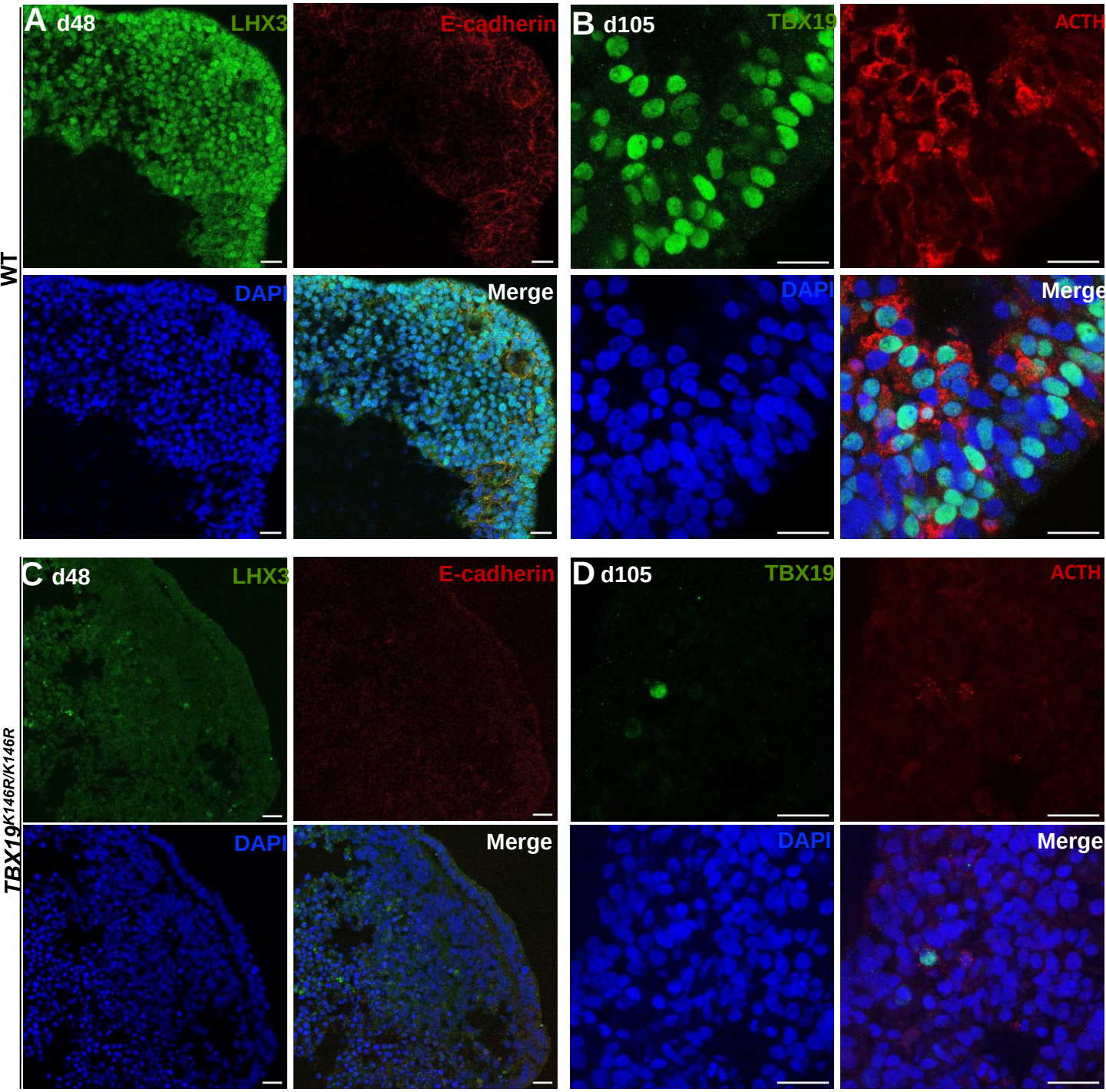
A d48
LHX3
E-cadherin
B d105
TBX19
ACTH
WT
DAPI
Merge
DAPI
Merge
C d48
LHX3
E-cadherin
D d105
TBX19
ACTH
TBX19K146R/K146R
DAPI
Merge
DAPI
Merge

Figure 3: Impairment of corticotroph development in *TBX19*$^{K146R/K146R}$ organoids as compared with control

A, C, Immunostaining of LHX3 and CDH1 (E-cadherin) expression in epithelial cells, typical of Rathke's pouch ectoderm in early pituitary primordia, was reduced in *TBX19*$^{K146R/K146R}$ organoids vs wild-type on day 48 (n=10 organoids for each group). Scale bars : 10 μm.

B, D, Immunostaining showed that ACTH and TBX19 expression was reduced in *TBX19*$^{K146R/K146R}$ organoids vs wild-type on day 105 (n=10 organoids for each group). Scale bars: 10 μm.

A WT organoid d105

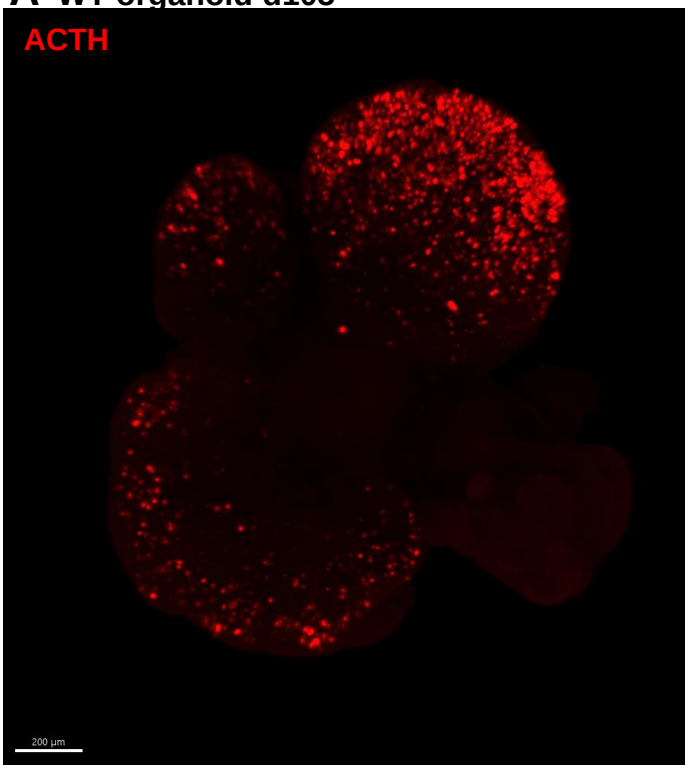

B *TBX19*$^{K146R/K146R}$ organoid d105

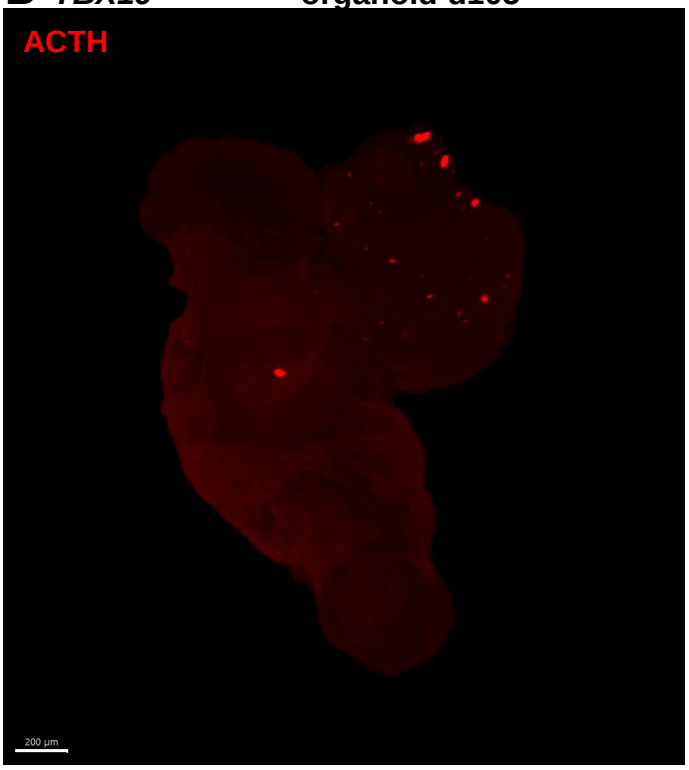

C

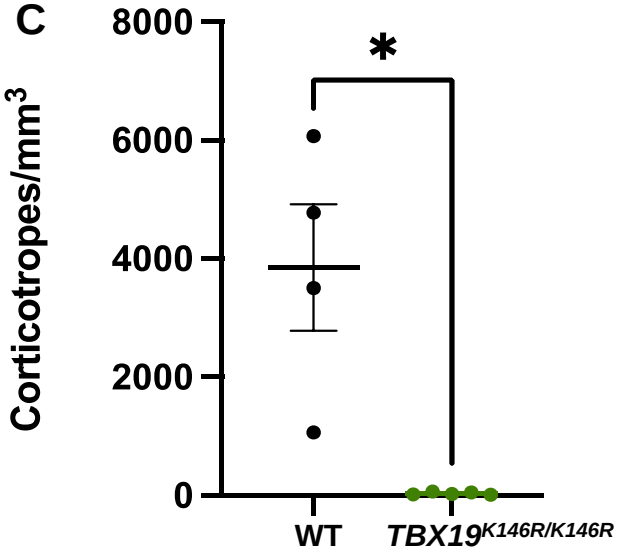

Figure 4: 3D reconstruction of whole Wild type (WT) and *TBX19*$^{K146R/K146R}$ organoids on day 105

A, A representative image of whole-mount immunostaining against ACTH in a cleared WT organoid on d105 using light-sheet microscopy. Scale bar: 200 μm.

B, A representative image of whole-mount immunostaining against ACTH in a cleared *TBX19*$^{K146R/K146R}$ organoid on d105 as above, showing impaired corticotroph differentiation. Scale bar: 200 μm.

C, The number of corticotroph cells per mm^3 was significantly decreased in *TBX19*$^{K146R/K146R}$ organoids (* p= 0.0159). Means ± *SEM* for n=4 WT, n=5 *TBX19*$^{K146R/K146R}$ organoids. Mann-Whitney test (unpaired, two-tailed, nonparametric).

A ***NFKB2* gene**

NFKB2^{D865G} **(GaC > GgC)**

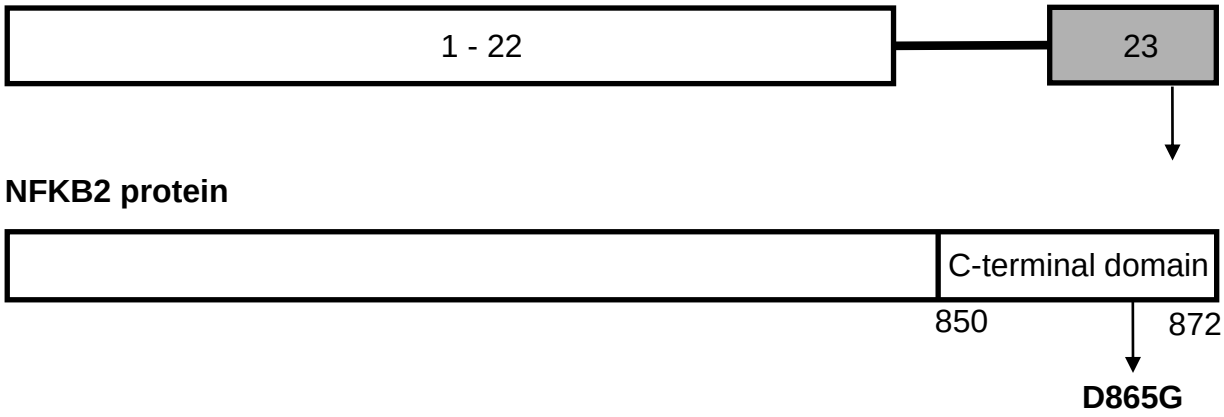

B **WT**

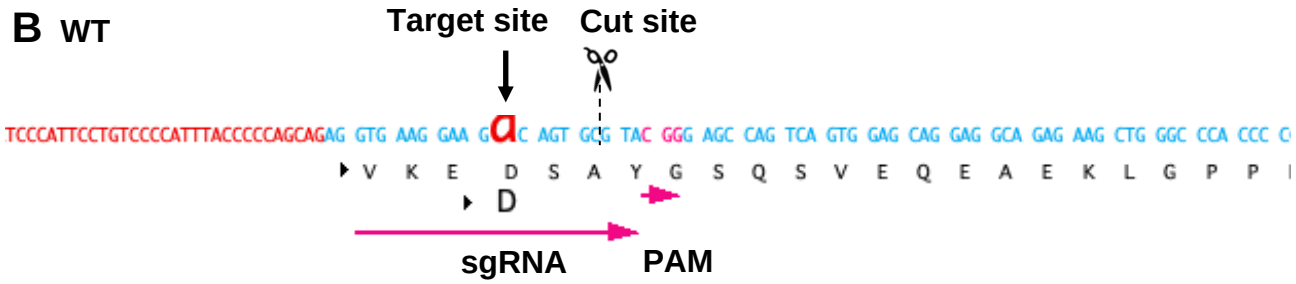

C **ssODN**

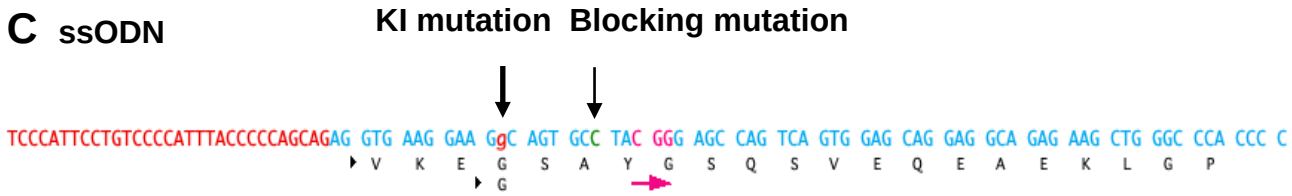

D

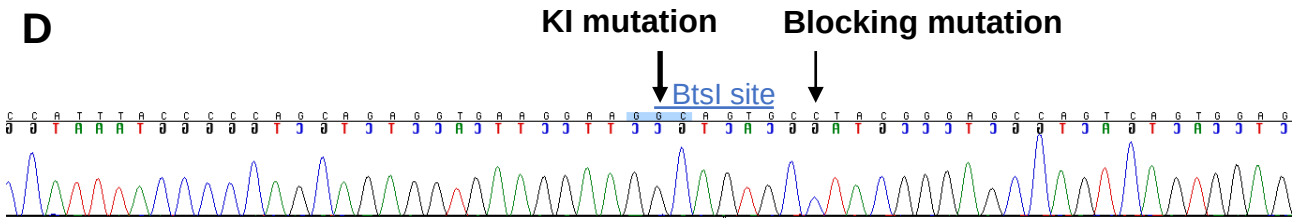

Figure 5: Design of sgRNA and ssODN to introduce a *NFKB2*^{D865G} mutation

A, Illustration of *NFKB2* gene (HGNC: 7795; Ensembl: ENSG00000077150; Human GRCh38) and NFKB2 protein.

B, WT sequence containing target site, cut site, target and PAM sequence.

C, ssODN design to introduce the missense mutation D865G into *NFKB2* using CRISPR/Cas9.

D, Sequence analysis of a representative *NFKB2*$^{D865G/D865G}$ hiPSC clone 7 obtained by Sanger sequencing after screening by CAPS. This clone was subsequently used in this work to differentiate into pituitary organoids (see below).

CAPS: cleaved amplified polymorphic sequences; hiPSC: human induced pluripotent stem cells; KI: knock-in; PAM: protospacer-adjacent motif; sgRNA: single guide RNA; ssODN: single-stranded oligo DNA nucleotides; WT: wildtype.

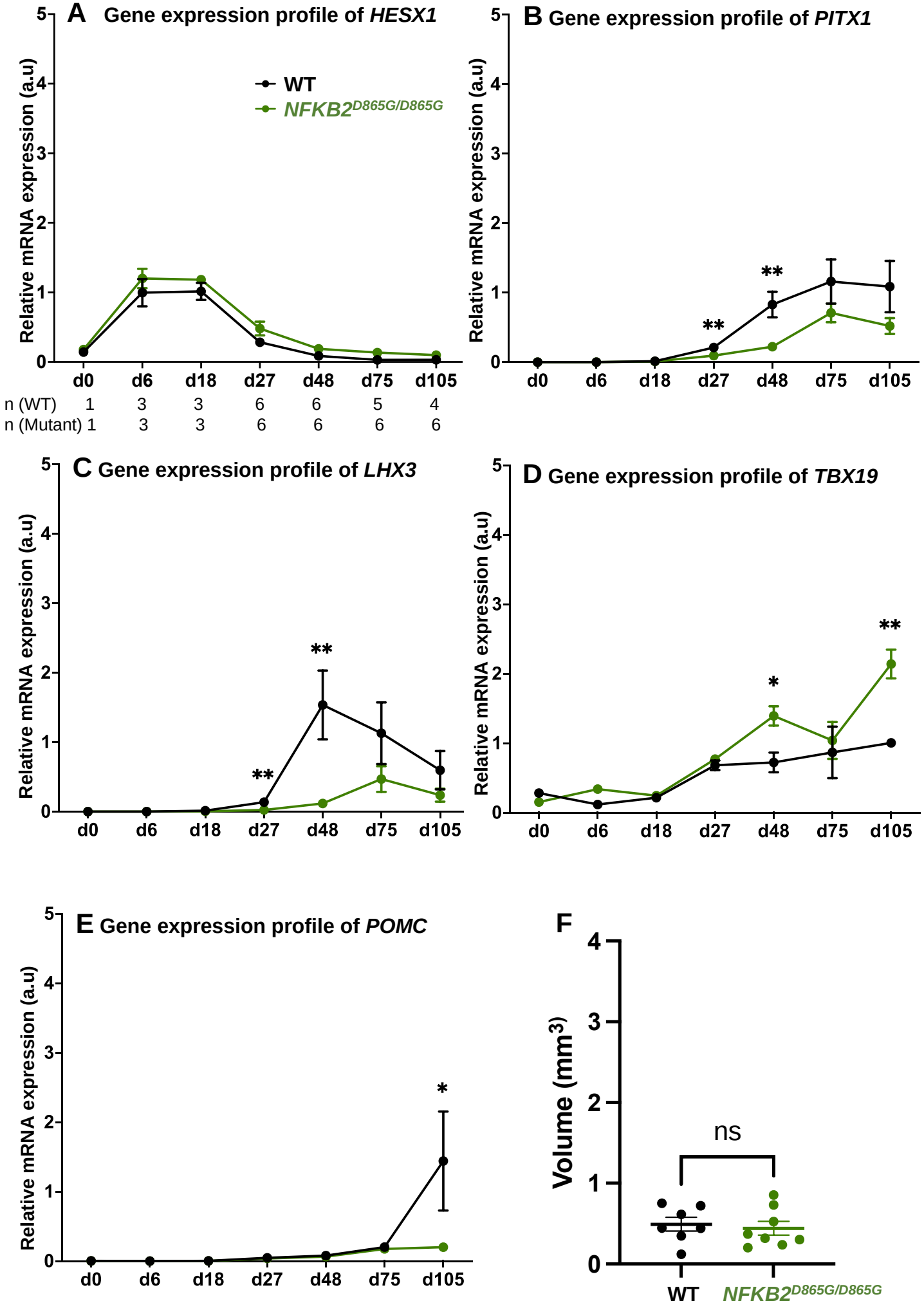
A Gene expression profile of HESX1
WT
NFKB2D865G/D865G
Relative mRNA expression (a.u)
d0 d6 d18 d27 d48 d75 d105
n (WT) 1 3 3 6 6 5 4
n (Mutant) 1 3 3 6 6 6 6
B Gene expression profile of PITX1
**
**
C Gene expression profile of LHX3
**
**
D Gene expression profile of TBX19
*
**
E Gene expression profile of POMC
*
F
Volume (mm3)
ns
WT
NFKB2D865G/D865G

Figure 6: **Time course of organoid growth and gene expression in WT and *NFKB2*$^{D865G/D865G}$ organoids**

A-E, Relative quantification (RQ) mRNA expression analysis for key markers of pituitary organoids during differentiation: WT (in black line) and *NFKB2*$^{D865G/D865G}$ organoids (in green line). Data show means ± standard error of the mean (SEM); n=1 on day (d)0, n=3 samples per group (8 organoids per sample) at the time points d6 and d18, n=4-6 organoids per group at each following time point (d27, d48, d75 and d105). Mann-Whitney t-test (unpaired, two-tailed, nonparametric). $p < 0.05$ (*), $p< 0.01$ (**).

A, Relative quantification expression of *HESX1*. The expression of *HESX1* was not significantly different in *NFKB2*$^{D865G/D865G}$ organoids vs. WT.

B, *PITX1* was significantly downregulated in *NFKB2*$^{D865G/D865G}$ organoids by d27 (** p= 0.0022) and d48 (* p= 0.0022).

C, *LHX3* was significantly lower in *NFKB2*$^{D865G/D865G}$ organoids as compared to WT on d27 (** p= 0.0087), and d48 (** p= 0.0087).

D, *TBX19* was significantly increased in *NFKB2*$^{D865G/D865G}$ organoids by d48 (* p= 0.026) and d105 (p= 0.0095).

E, *POMC* was significantly downregulated in *NFKB2*$^{D865G/D865G}$ organoids by d105 (* p= 0.019).

F, There was no significant difference in volume between WT and *NFKB2*$^{D865G/D865G}$ organoids (p= 0.6126). Data show means ± *SEM*; n=7 in the WT group, n=8 in the mutant group. Mann-Whitney test (unpaired, two-tailed).

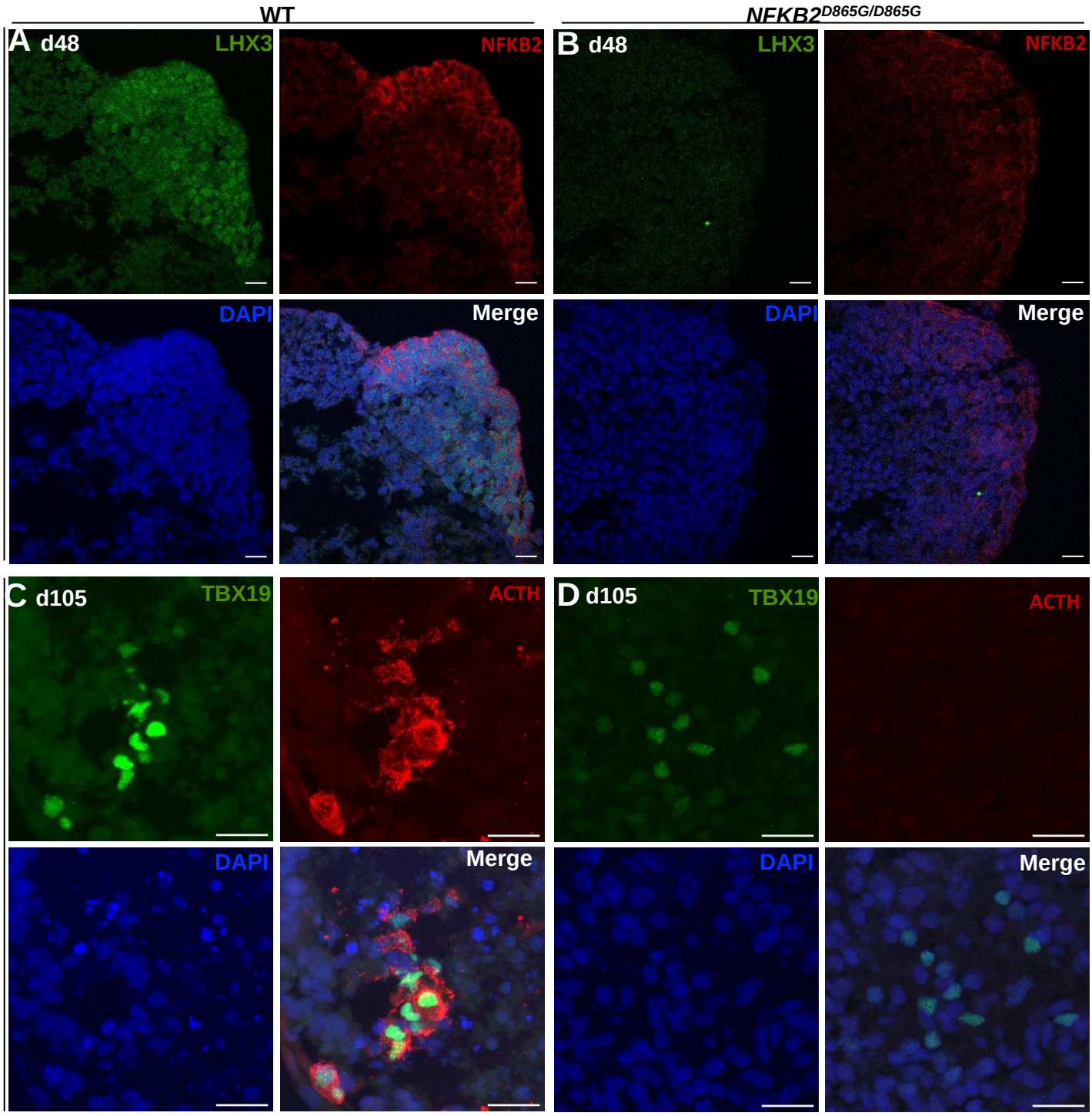
WT
NFKB2D865G/D865G
A d48
LHX3
NFKB2
DAPI
Merge
B d48
LHX3
NFKB2
DAPI
Merge
C d105
TBX19
ACTH
DAPI
Merge
D d105
TBX19
ACTH
DAPI
Merge

Figure 7: Impairment of pituitary development in *NFKB2*$^{D865G/D865G}$ organoids

A, B, Immunostaining of LHX3 and NFKB2 expression in the early pituitary-type epithelium was reduced in *NFKB2*$^{D865G/D865G}$ organoids vs WT on day 48 (n=10 organoids for each group). Scale bars: 10 μm

C, D, Immunostaining showed that by day 105, there was complete absence of corticotroph cells co-expressing ACTH and TBX19 in *NFKB2*$^{D865G/D865G}$ organoids versus WT organoids on day 105 (n=10 organoids for each group). Note the population of cells expressing TBX19 without ACTH in the mutant example. Scale bars: 10 μm

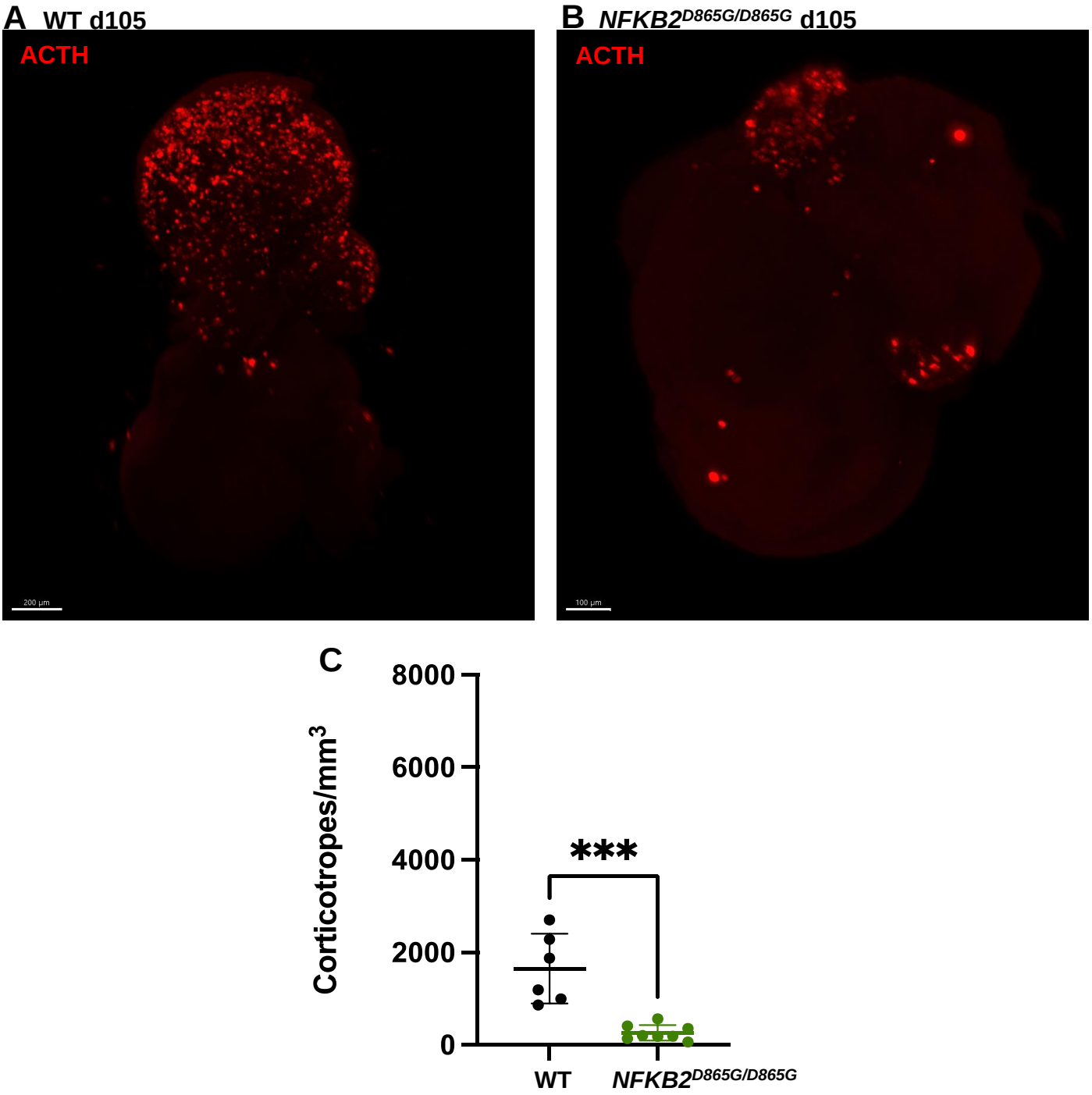
A WT d105
ACTH
200 µm
B NFKB2D865G/D865G d105
ACTH
100 µm
C
Corticotropes/mm3
8000
6000
4000
2000
0
***
WT
NFKB2D865G/D865G

Figure 8: **3D reconstruction of whole *NFKB2*$^{D865G/D865G}$ or WT organoids on day 105**

A, A representative image of whole-mount immunostaining against ACTH in a cleared WT organoid on d105 using light-sheet microscopy. Scale bar: 200 μm.

B, A representative image of whole-mount immunostaining against ACTH in a cleared *NFKB2*$^{D865G/D865G}$ organoid on d105 as above, showing impaired corticotroph differentiation. Scale bar: 100 μm.

C, The number of corticotroph cells per mm^3 was significantly decreased in *NFKB2*$^{D865G/D865G}$ organoids (* p= 0.0007). Means ± *SEM* for n=6 WT organoids, n=8 *NFKB2*$^{D865G/D865G}$ organoids. Mann-Whitney test (unpaired, two-tailed, nonparametric).

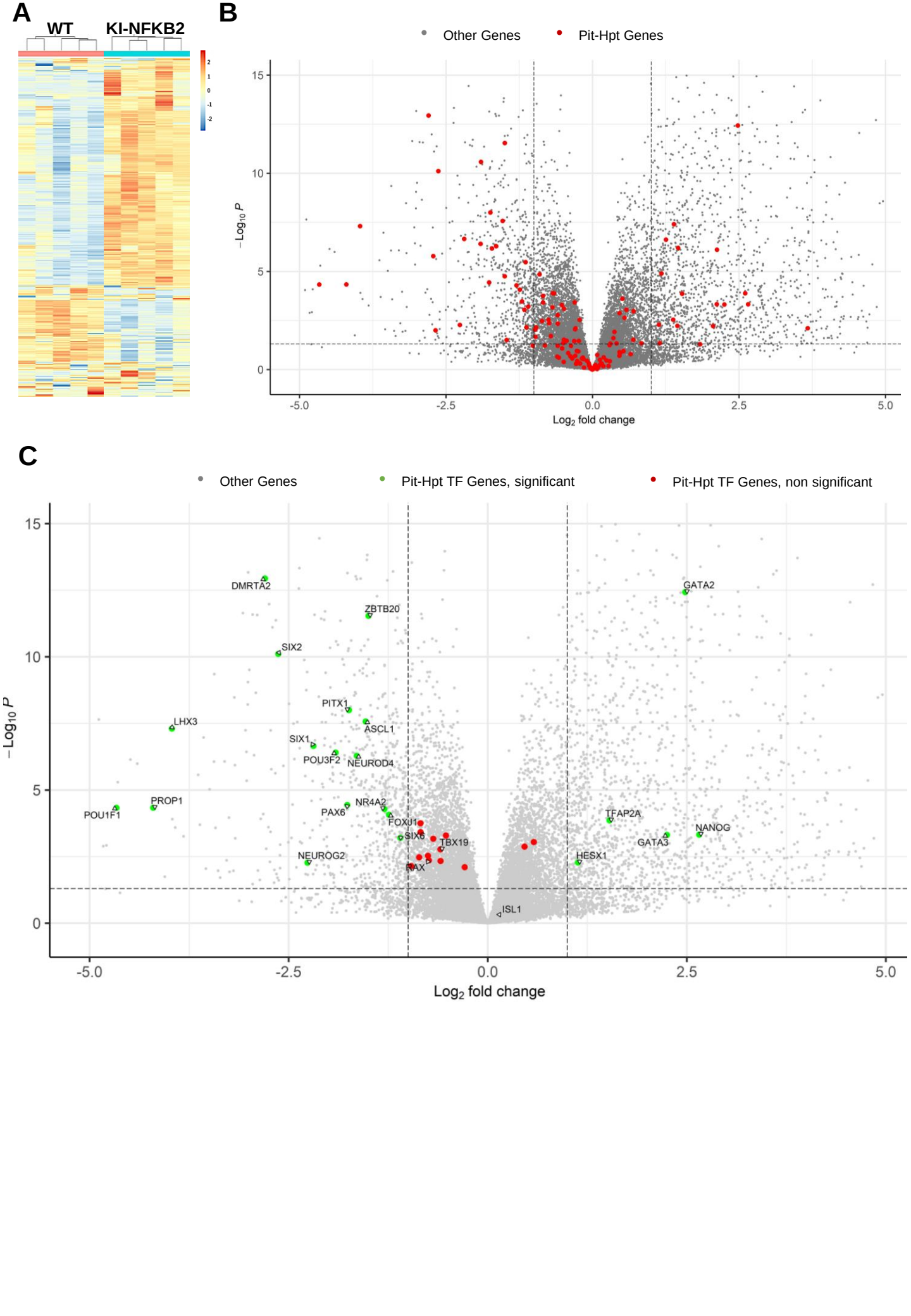
A
WT
KI-NFKB2
B
Other Genes
Pit-Hpt Genes
−Log10 P
Log2 fold change
C
Other Genes
Pit-Hpt TF Genes, significant
Pit-Hpt TF Genes, non significant
DMRTA2
ZBTB20
SIX2
PITX1
ASCL1
LHX3
SIX1
POU3F2
NEUROD4
PROP1
POU1F1
NR4A2
PAX6
FOXJ1
SIX6
TBX19
NEUROG2
RAX
ISL1
GATA2
TFAP2A
NANOG
GATA3
HESX1

Figure 9: **Whole transcriptome profiles of WT vs *NFKB2*$^{D865G/D865G}$ organoids on day 48**

A, Heat map showing global differential gene expression between WT and *NFKB2*$^{D865G/D865G}$ organoids (n=5 for each group).

B, Volcano plot of genes showing differential gene expression between WT and *NFKB2*$^{D865G/D865G}$ organoids. Red dots in the left panel indicate 143 genes involved in pituitary-hypothalamic development. Grey dots indicate all other genes detected in RNA-seq.

C, Volcano plot of genes showing differential gene expression between WT vs *NFKB2*$^{D865G/D865G}$ organoids. Green dots indicate genes coding for 21 key transcription factors (TF) whose expression is significantly changed (fold change < 0.5 or > 2, padj < 0.05). Red dots indicate fold change in expression between 0.5 and 2. Grey dots indicate all other genes detected in RNA-seq.

Pit-Hpt: pituitary-hypothalamic; KI: knock-in; TF: transcription factors

gene_name	FoldChange	padj	gene_name	FoldChange	padj	gene_name	FoldChange	padj
ADCYAP1	0,447	0,007888035	GNRHR	0,453	8,31212E-05	POLR3A	1,014	0,907184037
AIP	0,898	0,534416537	GNRHR2	0,698	0,239376773	POMC	0,434	0,003599837
ALDH1A2	0,152	4,59754E-05	GPR101	1,209	0,830451145	POU1F1	0,039	0,000715204
ALDH1A3	0,182	2,61E-13	GREB1	1,007	0,977843175	POU3F1	1,374	0,420928494
AR	0,634	0,001676979	GSX1	0,659	0,450115297	POU3F2	0,266	1,36281E-05
ARNT2	0,534	0,000269934	HES1	0,663	0,028047242	POU5F1	3,573	0,170177475
ASCL1	0,345	1,44E-06	HESX1	2,193	0,031209258	PROKR2	1,056	0,973652742
AXIN2	1,296	0,058892068	HEY1	0,804	0,130459101	PROP1	0,054	0,000712172
BMP2	0,750	0,342780888	HMGA2	0,775	0,194708366	RAX	0,599	0,026972637
BMP4	4,357	2,4368E-05	INHBB	0,458	0,039744399	RBPJ	0,814	0,046649215
BMPR1A	1,019	0,919913721	ISL1	1,097	0,758119581	S100B	0,304	2,15503E-05
BRAF	0,892	0,481826746	KDM1A	1,021	0,903369765	SALL1	1,106	0,761223759
CDH1	1,626	0,008999389	KRT8	2,617	1,99E-06	SHH	0,786	0,511785531
CGA	12,756	0,042344376	LATS1	0,857	0,019968707	SIX1	0,219	8,42E-06
CREB1	0,850	0,129014692	LATS2	1,460	0,016632236	SIX2	0,161	8,97E-09
CRH	4,347	0,004688935	LHX2	0,622	0,006247085	SIX3	0,859	0,699762446
CRHR1	0,156	0,051309993	LHX3	0,064	2,39E-06	SIX6	0,467	0,005859008
CRHR2	0,823	0,736016163	LHX4	0,557	0,003977929	SLC15A2	0,624	0,001635121
CTNNB1	1,009	0,955419302	MEN1	1,030	0,803086498	SLC6A3	2,215	0,157967352
CYP11A1	6,086	0,001655774	MSX1	0,904	0,909088208	SMO	0,957	0,7040106
DIO2	1,114	0,718852455	NANOG	6,301	0,004723205	SMOC2	4,163	0,034876305
DISP1	1,142	0,477079028	NEUROD1	0,883	0,509660164	SOX11	0,736	0,127568673
DLK1	0,594	0,019880505	NEUROD2	1,137	0,841778563	SOX2	0,815	0,421505197
DMRTA2	0,144	3,58E-11	NEUROD4	0,320	1,72108E-05	SOX3	0,787	0,501517696
DRD2	2,753	2,04541E-05	NEUROG1	0,493	0,192091391	SOX9	0,557	0,002135493
DUOX2	2,595	0,019613055	NEUROG2	0,208	0,031653158	SRD5A1	0,961	0,79794316
DZIP1	0,818	0,042643465	NFKB2	1,236	0,161439179	SST	0,994	0,992100441
EGR1	1,784	0,157681046	NKX2-1	0,707	0,15517589	SSTR1	0,509	0,090081721
ETS1	3,947	4,82E-13	NKX2-2	1,569	0,373223947	SSTR2	0,769	0,435993359
EYA1	0,514	0,039620927	NOG	1,376	0,318972037	TAZ	0,967	0,853180694
FGF10	0,267	3,49E-09	NOTCH1	1,006	0,98289259	TBX19	0,663	0,012939434
FGF2	1,224	0,182371108	NOTCH2	0,937	0,606914403	TBX3	0,997	0,989105106
FGF3	0,611	0,084446193	NR0B1	1,062	0,928929659	TCF4	1,015	0,957689002
FGF8	0,506	0,048269157	NR3C1	0,846	0,302794383	TCF7L2	1,178	0,588438732
FOLR1	2,729	0,034433598	NR4A1	1,227	0,621258008	TFAP2A	2,887	0,001732632
FOXA1	0,550	0,02192538	NR4A2	0,407	0,000780424	TGIF1	1,422	0,002776353
FOXC1	1,619	0,118175086	NR5A1	0,834	0,613961749	THRA	0,714	0,007115882
FOXJ1	0,424	0,001168862	NUPR1	1,384	0,347695524	THRB	2,260	0,000249134
FOXO1	1,494	0,007821304	OLFM1	0,830	0,291658503	TIPRL	0,810	0,003930719
FST	2,384	9,05E-06	OTP	0,663	0,193485664	TLE5	0,695	0,005015424
GATA2	5,579	9,69E-11	OTX1	0,863	0,722257262	TSHR	0,998	0,997529133
GATA3	4,758	0,004829173	OTX2	0,976	0,94712869	USP39	1,035	0,790802941
GHRH	0,712	0,650531144	PAX3	0,362	0,119629185	WNT4	0,712	0,116649738
GHRHR	0,672	0,485122167	PAX6	0,294	0,000592101	WNT5A	1,442	0,295426855
GLI1	1,050	0,841041925	PAX7	0,570	0,188199017	YAP1	1,091	0,565853991
GLI2	1,328	0,159304929	PCSK1	0,354	0,000327177	ZBTB20	0,354	5,29E-10
GLI3	1,279	0,10094389	PITX1	0,299	6,27E-07	ZEB2	1,378	0,010775016
GNAS	1,058	0,395187491	PITX2	1,072	0,86688154			

Table 1: RNA-seq expression data for a list of 143 genes known to have a functional influence on pituitary-hypothalamic development. Differentially expressed genes (padj < 0.05) in *NFKB2*$^{D865G/D865G}$ organoids are highlighted in green.